

# Carbon and Strontium Abundances of Metal-Poor Stars<sup>1</sup>

David K. Lai

*University of California Observatories/Lick Observatory, Department of Astronomy and Astrophysics, University of California, Santa Cruz, CA.*

Jennifer A. Johnson

*Department of Astronomy, Ohio State University, Columbus, OH.*

Michael Bolte

*University of California Observatories/Lick Observatory, Department of Astronomy and Astrophysics, University of California, Santa Cruz, CA.*

and

Sara Lucatello

*Osservatorio Astronomico di Padova, Vicolo dell'Osservatorio 5, 35122 Padua, Italy.*

david@ucolick.org, jaj@astronomy.ohio-state.edu, bolte@ucolick.org,  
sara.lucatello@oapd.inaf.it

## ABSTRACT

We present carbon and strontium abundances for 100 metal-poor stars measured from  $R \sim 7000$  spectra obtained with the Echellette Spectrograph and Imager at the Keck Observatory. Using spectral synthesis of the G-band region, we have derived carbon abundances for stars ranging from  $[\text{Fe}/\text{H}] = -1.3$  to  $[\text{Fe}/\text{H}] = -3.8$ . The formal errors are  $\sim 0.2$  dex in  $[\text{C}/\text{Fe}]$ . The strontium abundance in these stars was measured using spectral synthesis of the resonance line at  $4215 \text{ \AA}$ . Using these two abundance measurements along with the barium abundances from our previous study of these stars, we show it is possible to identify neutron-capture-rich stars with our spectra. We find, as in other studies, a large

---

<sup>1</sup>The data presented herein were obtained at the W.M. Keck Observatory, which is operated as a scientific partnership among the California Institute of Technology, the University of California and the National Aeronautics and Space Administration. The Observatory was made possible by the generous financial support of the W.M. Keck Foundation.

scatter in  $[C/Fe]$  below  $[Fe/H] = -2$ . Of the stars with  $[Fe/H] < -2$ ,  $9 \pm 4\%$  can be classified as carbon-rich metal-poor stars. The Sr and Ba abundances show that three of the carbon-rich stars are neutron-capture-rich, while two have normal Ba and Sr. This fraction of carbon enhanced stars is consistent with other studies that include this metallicity range.

*Subject headings:* Abundances — stars, carbon — stars, nuclear reactions, nucleosynthesis, abundances — stars, Population II — stars

## 1. Introduction

The study of metal-poor stars has evolved in the past twenty years from the close examination of the few known stars with  $[Fe/H] < -3.0$  to the investigation of the statistical properties of large samples of very metal-poor stars. This new wealth of stars with low  $[Fe/H]$ , originally discovered in the surveys of Bond (1980) and Beers et al. (1992) (hereafter, BPS), and more recently in new surveys, including the Hamburg/ESO Survey (Christlieb et al. 2002b) and SDSS (Beers et al. 2006), has revealed a number of subgroups among the metal-poor stars characterized by different abundance patterns. These include stars with large enhancements of elements made by the r-process (e.g., McWilliam et al. 1995; Hill et al. 2002) and stars with large enhancements in the  $\alpha$ -elements (Aoki et al. 2002a). Among the most prominent types are the carbon-rich objects (here we define C-rich as  $[C/Fe] \geq 1$ ). As increasing numbers of C-rich stars were studied, it became clear that the abundances of other elements could vary widely from one C-rich star to another. Beers & Christlieb (2005) classified these objects into four subclasses based on the abundances of the heavy neutron-capture elements Ba and Eu: CEMP-r, CEMP-s, CEMP-r/s and CEMP-no. The CEMP-r objects have enhanced Ba and a low  $[Ba/Eu]$  ratios that suggest solely a r-process contribution, while the CEMP-s and CEMP-r/s also have enhanced Ba, but higher  $[Ba/Eu]$  ratios which suggest that the s-process has polluted them only (-s) or as well (-r/s). The CEMP-no stars show no enhancement in Ba or Eu.

One of the goals of current research on metal-poor stars is to quantify the ratios of the different types of C-rich stars as a function of  $[Fe/H]$ . This will isolate those phenomena associated with the early Universe and test whether certain types of events were more common. An example of the former are the extremely large  $[C/Fe]$  abundances found in the two most  $[Fe/H]$ -poor stars (Christlieb et al. 2002a; Frebel et al. 2005). An example of the latter may be the higher fraction of stars at low  $[Fe/H]$  that show signs of carbon mass transfer from an asymptotic giant branch (AGB) companion.

Another important quantity is the the overall fraction of C-rich stars, as a measure of the frequency of carbon pollution events. The percentage of C-rich stars increases as  $[\text{Fe}/\text{H}]$  decreases (Lucatello et al. 2006; Rossi et al. 2005), going up to 100% at  $[\text{Fe}/\text{H}] < -5$ . However, the total fraction of CEMP stars at low metallicities is in dispute. Estimates range from 25% for  $[\text{Fe}/\text{H}] < -2.5$  (Marsteller et al. 2005) to  $14 \pm 4\%$  for  $[\text{Fe}/\text{H}] < -2.0$  (Cohen et al. 2005) to  $9 \pm 2\%$  for the same metallicity range in Frebel et al. (2006). Lucatello et al. (2006) found a lower limit of  $21 \pm 2\%$  for the fraction of stars with  $[\text{Fe}/\text{H}] < -2.0$  that are C-rich in the HERES sample (Barklem et al. 2005). Possible reasons for the discrepancies between studies include underestimates in some surveys of the  $[\text{Fe}/\text{H}]$  for stars with strong CH/CN molecular features (Cohen et al. 2005), trends in the fraction of C-rich stars with distance from the Galactic plane (Frebel et al. 2006), and the inclusion in samples of giants whose C abundance has been decreased because evolutionary dilution (Lucatello et al. 2006) and/or has been processed some of their carbon through the CN cycle (Aoki et al. 2007). Therefore, increasing the sample size of metal-poor stars with C-abundances, especially for stars with warmer atmospheres that are the least likely to suffer from most of the above effects, is important for improving statistics at the edge of the metallicity distribution function.

The other goal of this study is to further constrain the evolution of neutron-capture elements, specifically by comparing measured abundances for the light neutron-capture element Sr, with the heavy neutron-capture element Ba. By examining the light neutron-capture elements, Sr-Y-Zr, it has been shown that there must be a distinct neutron-capture process besides the classical s- and r-processes that contributes to their abundances (e.g. McWilliam 1998) A likely source for some of this production is the weak s-process in more metal-rich stars (e.g. Truran et al. 2002; Burris et al. 2000), but to fully understand the abundances, Travaglio et al. (2004) suggest that there needs to be another production site which is unrelated to the weak s-process that they call LEPP (lighter element primary process). It is important to obtain more measurements of  $[\text{Sr}/\text{Ba}]$  to further constrain the magnitude of these processes, as well as where it provides the greatest contribution. This is particularly relevant for the CEMP stars, because, as mentioned previously, they display a wide variety in the abundance ratios of the heavy elements.

Previous high-resolution studies, e.g. McWilliam (1998), Burris et al. (2000), Aoki et al. (2005), and Barklem et al. (2005) explored this ratio for a number of stars in the metal-poor regime. In this study we show it is possible to obtain this ratio from relatively low-resolution spectra.

We report on the carbon and strontium abundances for 100 stars, which are most of the sample of Lai et al. (2004) (hereafter, Paper I). While this sample is biased toward metal-poor stars, it does not suffer from substantial biases in  $[\text{C}/\text{Fe}]$  ratios among the warmer stars.

It extends to higher metallicities than other studies, which allows us to observe trends in number of C-rich stars with  $[\text{Fe}/\text{H}]$ . We can pair  $[\text{C}/\text{Fe}]$  and  $[\text{Sr}/\text{Fe}]$  measurements with the Ba abundances from Paper I and place these stars into their CEMP subclasses. Preliminary measurements of the carbon abundances for this sample were used to identify two stars for higher resolution follow-up: CS 22183-015 (Johnson & Bolte 2002a) and CS 31062-050 (Johnson & Bolte 2004).

## 2. Observations, Sample Selection and Reductions

The details of the observations and reduction procedures are presented in Paper I; we present only an outline here. The goal of Paper I was to measure  $[\text{Fe}/\text{H}]$  and abundance ratios in a large number of metal-poor candidates. The candidates were selected from four sources: Norris et al. (1999), Anthony-Twarog et al. (2000), (Allende Prieto et al. 2000) and the original BPS paper. We attempted to select the most metal-poor candidates from each survey. For Anthony-Twarog et al. (2000), Allende Prieto et al. (2000), and BPS, we selected candidates based on their  $[\text{Fe}/\text{H}]$  estimates. For Norris et al. (1999), our selection was based on the UBV excess. For this paper we restrict our carbon measurements to the objects from Paper I with  $[\text{Fe}/\text{H}] < -1.3$  because the metallicity and atmosphere determinations are uncertain for higher metallicities. We note that the spectrum for CS30332-067 was misidentified in our Paper I, and is therefore excluded here. This yielded a total of 100 objects for this study.

We obtained our spectra over the course of several runs using the Echellette Spectrograph and Imager (ESI) (Sheinis et al. 2002) at the Keck 2 telescope. We ran ESI in the echellette mode with the  $0''.75$ -wide slit, resulting in a spectral resolution of  $R \simeq 7000$ . The wavelength coverage of the spectra easily encompasses the G-band region used in our analysis. We then used IRAF<sup>1</sup> to extract the spectra to one-dimensional, wavelength calibrated, continuum-divided form.

---

<sup>1</sup>IRAF is distributed by the National Optical Astronomy Observatories, which are operated by the Association of Universities for Research in Astronomy, Inc., under cooperative agreement with the National Science Foundation.

### 3. Abundance Analysis

With the relatively low resolution of ESI, only the resonance lines of Sr could be detected. We derived the Sr abundance for our sample via synthesis of the SrII line at 4215 Å. We used the  $\log gf$  value from Ivans et al. (2006), and the linelist from Kurucz & Bell (1995) for the surrounding lines in the region along with the LTE spectrum synthesis and analysis program MOOG (Snedden 1973), for the spectrum synthesis. Unfortunately the SrII 4077 Å line proved unsuitable because of blending with the 4077.3 Å LaII line and 4078.0 Å DyII line, both elements that we cannot measure independently in our spectra. Figure 1 shows a sample synthesis of the 4215 Å line in the star CS 22957-022. It is clear that the moderate resolution of ESI makes spectral synthesis necessary to measure Sr accurately. In particular we must ensure to take the Fe and CH blends into account.

The carbon abundances were determined by spectral synthesis of the 4300 Å region of the spectrum, which encompasses the  $A^2\Delta-X^2\Pi$  transitions of CH. We used the linelist from Lucatello et al. (2003) and MOOG for the spectral synthesis.

Atmospheric parameters and models were taken directly from Paper I. We arbitrarily assumed a value of 10 for the  $^{12}\text{C}/^{13}\text{C}$  ratios. The resolution of the spectra prevented us from performing measurements of this ratio. The effects of this choice are discussed § 3.0.2. Figure 2 shows a sample of the synthesis.

The relatively low resolution of ESI also affects the sensitivity we have to measuring carbon abundances. To test this effect we ran a set of trial synthesis ranging from 4600 to 6500 K and with surface gravities determined from the isochrones of Bergbusch & Vandenberg (1992). The metallicity of the models were all set to  $[\text{Fe}/\text{H}]$  of  $-2.5$ . For our range of temperatures, there are generally two possible choices for the surface gravity, either along the main sequence or on the giant/subgiant branch. We calculated the lower limits of  $[\text{C}/\text{Fe}]$  that we can measure for both cases and plot them in Figure 3.

There are four main components to the carbon abundance error. Uncertainties in the synthesis fit, uncertainties in the atmospheric parameters, errors in the atomic line parameters, and, for C, unknown  $^{12}\text{C}/^{13}\text{C}$  ratios all contribute to the final abundance uncertainty.

The uncertainty due to the synthesis fit was estimated by using the values of the largest and smallest carbon abundance that could fit the data by eye. Figure 2 shows an example of these sample fits. The typical fitting error was between 0.1 to 0.2 dex.

### 3.0.1. *Errors due to uncertainties in the adopted atmosphere parameters*

We used three stars to represent the errors for objects in different stages of evolution, BD+02 3375, CS 22183-031, and BS 16928-053. We then varied the atmospheric parameters,  $T_{\text{eff}}$ ,  $\log g$ ,  $[\text{Fe}/\text{H}]$ , and  $\xi$ , for each of these stars to determine the effect on the  $[\text{C}/\text{Fe}]$  and  $[\text{Sr}/\text{Fe}]$  measurements. The results are presented in Tables 1 and 2. The results of varying  $[\text{M}/\text{H}]$  in the atmospheres proved negligible in the final abundance measurements. We also took into account the  $T_{\text{eff}}$ -  $\log g$  cross term. Varying  $T_{\text{eff}}$  by +125 K,  $\log g$  changes by  $-0.03$ ,  $0.15$ , and  $0.29$  dex for BD+02 3375, CS 22183-031, and BS 16928-053, respectively.

### 3.0.2. $^{12}\text{C}/^{13}\text{C}$

The resolution of ESI prevented us from carrying out measurements of the  $^{12}\text{C}/^{13}\text{C}$  ratio. We instead used a value of 10 for the entire sample when measuring the total carbon abundance. This is likely an incorrect assumption, so we chose the same three stars used for the atmospheric error analysis to test the consequences of this assumption. We chose two extreme values of  $^{12}\text{C}/^{13}\text{C}$ , 4 and 200, and ran the synthesis again. The effect was negligible for the high case. The  $[\text{C}/\text{Fe}]$  changed by less than  $+0.05$  dex in all three cases, a level that is not detectable in our spectra. Using the lower ratio value,  $^{12}\text{C}/^{13}\text{C}$  set to 4, the  $[\text{C}/\text{Fe}]$  changed by  $-0.05$ ,  $-0.1$ , and  $-0.1$  dex for BD+02 3375, CS 22183-031, and BS 16928-053, respectively.

This comes about because the  $^{13}\text{CH}$  does not contribute significantly to the absorption until it is a very high fraction of the overall carbon abundance. The effect is that we are only sensitive to  $^{12}\text{CH}$  if we assume  $^{12}\text{C}/^{13}\text{C}$  greater than 10 for our stars. Because of the resolution of our spectra, having a low  $^{12}\text{C}/^{13}\text{C}$  does not noticeably change the shape of the molecular feature, but it does change the depth. If the true value of  $^{12}\text{C}/^{13}\text{C} \simeq 4$ , then we have increased and hence overestimated the overall carbon abundance to match the observations. Therefore if the stars are heavily mixed compared to what was assumed (very low  $^{12}\text{C}/^{13}\text{C}$ ) then we may be overestimating  $[\text{C}/\text{Fe}]$  by 0.1 dex. This is only likely for the coolest giants in our sample,  $T_{\text{eff}} \leq 4800$  K, where deep mixing has likely taken place enough to appreciably lower the  $^{12}\text{C}/^{13}\text{C}$  (Cayrel et al. 2004).

### 3.0.3. *Total uncertainty*

The total error for our  $[\text{C}/\text{Fe}]$  values is taken to be the quadrature sum of the atmospheric and fitting error for each object. The contribution from uncertainty of the  $^{12}\text{C}/^{13}\text{C}$  ratio is

not included since we assume that it is negligible in most of our stars, although it may be a systematic offset for our coolest giants. As shown in Table 3, we find errors ranging from 0.17 to 0.26 dex.

The total error on our  $[\text{Sr}/\text{Fe}]$  measurements is taken to be the quadrature sum of the atmospheric error for the stellar parameters closest to each star, and 0.2 dex, the typical fitting error of the synthesis. This corresponds to errors of 0.31, 0.32, and 0.39 dex for dwarfs, subgiants/turn-off stars, and giants, respectively. These relatively large errors are a consequence of using a strong resonance line of SrII with its high sensitivity to the choice of microturbulent velocity.

### 3.1. Comparisons with Previous Studies

We compared our results for  $[\text{C}/\text{Fe}]$  with previously determined values for 20 stars. We list these comparison values in Table 4 and plot them in Figure 4. The dispersion between our study and the previous values is 0.21 dex, with a mean offset of -0.03 dex in the sense of our values minus previous values. This is consistent with our errors.

Table 5 lists our values for  $[\text{Sr}/\text{Fe}]$  and previously measured values of  $[\text{Sr}/\text{Fe}]$ . From Figure 5 we can see that our  $[\text{Sr}/\text{Fe}]$  measurements are higher than previous studies. Although we have attempted to properly take into account all of the blends that would affect our SrII line, this suggests that either we have neglected to take into account a line/lines that do not affect the high-resolution studies, or we are not treating the known blends (e.g. the FeI line shown in Figure 1) accurately. Also, comparing our stellar parameters with those from the studies listed in Table 5, we find that our  $\log g$  values are on average 0.36 dex lower, while the  $T_{\text{eff}}$  and microturbulent velocities show no offset. As indicated in Table 2, this means we may be deriving  $[\text{Sr}/\text{Fe}]$  values that are 0.05 to 0.1 dex too high. The average offset between our measurements and those from the earlier studies is 0.21 dex, a part of which that may be explained by our  $\log g$  discrepancy. However the scatter of the  $\Delta[\text{Sr}/\text{Fe}]$  values is a relatively low 0.14 dex. We are in excellent agreement with previous measurements if we subtract off this average offset. It may be appropriate then, to lower our measured  $[\text{Sr}/\text{Fe}]$  values by 0.21 dex when comparing our results with those from high resolution studies.

There are three studies that were not included in the above comparisons. Two of these included the stars HD 115444 and HD 122563. Johnson & Bolte (2002b), measured  $[\text{Sr}/\text{Fe}]$  as  $-0.27$  and  $-0.39$  for HD 115444 and HD 122563, as compared to our measured values of 0.26 and  $-0.06$ . For both these differences fall within the quoted errors assuming the 0.2 dex offset, but only barely. The main reason for these differences is that the atmospheric

parameters adopted for both stars in Johnson & Bolte (2002b) are quite different from those used in this study. Using their model atmosphere parameters and our measurements, we find  $[\text{Sr}/\text{Fe}]$  values lowered to 0.06 and  $-0.16$ , for HD 115444 and HD 122563, respectively. Similarly, Cohen et al. (2004) find  $[\text{Sr}/\text{Fe}] = 0.06$  for BS 16945-054 compared to our value of  $-0.32$ . However, if we adopt their atmospheric parameters our measurement gives  $[\text{Sr}/\text{Fe}] = -0.07$ .

The third study, by Westin et al. (2000) gives  $[\text{Sr}/\text{Fe}]$  of 0.32 and 0.17 for HD 115444 and HD 122563, respectively. Both of these values are greater than our measurements, which is at odds with the other comparison results summarized in Table 5. In addition the Westin et al. (2000) HD 122563 and HD 115444  $[\text{Sr}/\text{Fe}]$  values are much higher than the abundances from Honda et al. (2006) and Honda et al. (2004). Unlike the case for Johnson & Bolte (2002b), the atmospheric parameters for both stars from Westin et al. (2000), the studies just listed, and ours study are in reasonable agreement, so it is unclear why the Westin et al. (2000) abundances are different. Although we have chosen to use the Honda et al. (2006) and Honda et al. (2004) values for our comparisons above, it should be noted that the Westin measurements taken by themselves are entirely consistent with our abundances. If we did adopt the Westin values, we would find an overall offset of 0.16 dex from previous studies, and a scatter of 0.20 dex in  $\Delta[\text{Sr}/\text{Fe}]$ .

#### 4. Results

Table 3 summarizes our values for  $[\text{Sr}/\text{Fe}]$  and  $[\text{C}/\text{Fe}]$  relative to the solar abundances of Anders & Grevesse (1989), along with the fitting, atmosphere, and final errors for  $[\text{C}/\text{Fe}]$ . Figure 6 shows  $[\text{C}/\text{Fe}]$  plotted against  $[\text{Fe}/\text{H}]$ ,  $T_{\text{eff}}$ , and  $\log g$ . We see a trend of decreasing  $[\text{C}/\text{Fe}]$  with decreasing  $T_{\text{eff}}$  beginning at 5000 K, which is also mirrored by the  $\log g$  plot. This is consistent with the results of Cayrel et al. (2004) where in giants deep mixing has brought material to the surface from layers where carbon has been converted to nitrogen (Gratton et al. 2000). Unfortunately we cannot obtain nitrogen abundances from our spectra to verify this in our stars, as was done by Spite et al. (2005) for the Cayrel sample.

There is a large scatter over the entire sample with a dispersion of 0.52 dex. The average for  $[\text{C}/\text{Fe}]$  over the entire sample is 0.11 dex. Below  $[\text{Fe}/\text{H}] = -2.0$  we note that the scatter is 0.59 dex, compared to only 0.33 dex for more metal-rich objects. This reflects the fact that all extremely high  $[\text{C}/\text{Fe}]$  values are found for  $[\text{Fe}/\text{H}] < -2.0$ . Considering only stars with  $[\text{Fe}/\text{H}] < -2.0$ , we find that 5 out of 53 stars, or  $9 \pm 4\%$  (assuming a bimodal distribution), can be classified as CEMP stars among the entire sample. If we confine the sample to stars with  $T_{\text{eff}} > 5200\text{K}$ , which we argue below represent a sample unbiased in C-richness, we find



3 out of 26 stars, or  $12\pm 6\%$  fall into the CEMP category.

Figure 7 shows how  $[\text{Sr}/\text{Fe}]$  varies over  $[\text{Fe}/\text{H}]$ ,  $T_{\text{eff}}$ , and  $\log g$ . There are no obvious trends with  $T_{\text{eff}}$  or  $\log g$ . As has been seen in previous studies (e.g. McWilliam et al. (1995)), there does appear a marked increase in the scatter of  $[\text{Sr}/\text{Fe}]$  below  $[\text{Fe}/\text{H}]\simeq -2.3$ , as well as an increase in the number of very low  $[\text{Sr}/\text{Fe}]$  abundance measurements. This reflects the inhomogeneity of the early ISM and the stochastic nature of the neutron-capture process that produced Sr.

## 5. Discussion

### 5.1. Sr in the early Galaxy

Combining our Sr abundances with Ba abundances from Paper I allows us to see the evidence of different neutron-capture events in an individual star. We show this in Figures 8 and 9. The three stars with the highest values of  $[\text{Ba}/\text{Fe}]$ , CS 22183-015 (Johnson & Bolte 2002a), CS 31062-050 (Johnson & Bolte 2004), and CS22898-027 (McWilliam et al. 1995), have been shown to be heavily polluted by s-process material. The square symbols mark the stars known to have an r-process signature; HD 115444 (Westin et al. 2000), BS 16981-009 (also called HE1430+0053, Barklem et al. 2005), CS 22183-031 (Honda et al. 2004), CS 22892-052 (Snedden et al. 1996, 2003), and CS31082-001 (Hill et al. 2002). Six of eight of these stars appear separated from the majority of the points in Figures 8 and 9. The two exceptions are HD 115444 and CS 22183-031. They have neither a high  $[\text{Ba}/\text{Fe}]$ , nor particularly low  $[\text{Sr}/\text{Ba}]$ . Using lower resolution spectra, we can identify highly r/s-process enhanced stars, but we would not be complete in doing so.

The scatter of our  $[\text{Sr}/\text{Ba}]$  values at  $[\text{Fe}/\text{H}] > -2.2$  is 0.29, well within our errors. At  $[\text{Fe}/\text{H}] \leq -2.2$ , however, the scatter is 0.55 dex. This indicates that multiple processes are contributing to the light neutron-capture synthesis. As is clearly seen in figure 8 many of our stars are measured at or above  $[\text{Sr}/\text{Ba}]=0$ , far from where the main s- and main r-process enhanced stars sit. This demonstrates that in the early galaxy Sr was being produced in some other process, whether it was a weak s- or r-process (Johnson & Bolte 2002b; Kratz et al. 2007), or some other unidentified process (Travaglio et al. 2004). In particular EMP stars such as BS 16550-087, with a  $[\text{Sr}/\text{Ba}]$  of 1.78, may prove ideal for testing different scenarios for Sr production.

## 5.2. Classification of the C-rich stars

The Ba abundances also allow us to place the CEMP stars into subclasses. We plot  $[\text{Ba}/\text{Fe}]$ , derived in Paper I, versus  $[\text{C}/\text{Fe}]$  in figure 10. The three stars in the upper right hand corner of the plot all have follow-up data from which Eu could be measured, revealing that CS 22183-015, CS 31062-050, and CS 22898-027 (Aoki et al. 2002c) are CEMP-r/s stars.

The object CS 22892-052 has also been labeled in figure 10. As detailed by Sneden et al. (1996, 2003), this is a very r-process-rich object that is also carbon-rich (CEMP-r). With a few exceptions CS 22892-052 fits the scaled solar system r-process abundance extremely well, suggesting that its barium abundance has a predominately r-process origin. This has been the only CEMP and r-process-rich star yet discovered (Ryan et al. 2005), and it suggests that the carbon over-abundance is not connected to it’s high barium abundance. This is also a way to differentiate r and s-process stars if a high  $[\text{Ba}/\text{Fe}]$  is measured, even when a r-process element such as europium is not measured. As all other r-process enhanced EMP stars, such as CS 31082-001, are not C-rich then a high  $[\text{Ba}/\text{Fe}]$  with normal  $[\text{C}/\text{Fe}]$  is an indication of r-process and not s-process enhancement.

Three stars in figure 10 have  $[\text{C}/\text{Fe}] \geq 1$ , but  $[\text{Ba}/\text{Fe}] < 0$ : BS 16077-007 with  $[\text{Fe}/\text{H}] = -2.8$ , BS 16929-005 with  $[\text{Fe}/\text{H}] = -3.3$  and CS 29502-092 with  $[\text{Fe}/\text{H}] = -2.9$ . The lack of Ba indicates that these stars have not been polluted by a large s-process (or the r/s process) event, and a different mechanism must have taken place to explain their C-enhancement. An extreme example of this type of object is CS 22957-027, analyzed by Norris et al. (1997), with  $[\text{C}/\text{Fe}] = 2.2$  and  $[\text{Ba}/\text{Fe}] = -1.0$ . According to Paper I, BS 16077-007 has  $[\text{Mg}/\text{Fe}] = 0.21$ , BS 16929-005 has  $[\text{Mg}/\text{Fe}] = 0.63$ , and CS 29502-092 has  $[\text{Mg}/\text{Fe}] = 0.42$  dex. BS 16929-005 has also been observed by Honda et al. (2004), who measured a  $[\text{Mg}/\text{Fe}]$  of 0.38 dex. CS 29502-092 was also observed by Aoki et al. (2002b) with much higher resolution, giving results consistent with ours. Therefore, these stars are not enriched in the  $\alpha$  elements as well as C, and are not members of the same class as CS 29498-043, which has high  $[\text{C}/\text{Fe}]$ , low  $[\text{Ba}/\text{Fe}]$ , but a  $[\text{Mg}/\text{Fe}] = 1.81$  (Aoki et al. 2002a). One possibility is that these objects are the result of stellar formation from carbon-rich gas. Or, as suggested by Norris et al. (1997), it could come from a mechanism described by Fujimoto et al. (2000) where a helium core flash in a zero metal star induces hydrogen burning, and the subsequent material is then dredged up to the surface layers.

Overall, our sample seems to fall into three classes. Using the designation of Ryan et al. (2005), there are two classes of carbon-rich metal-poor stars, one that is rich in the s-process and one that is normal in the s-process. Then there are the barium and carbon ‘normal’ objects that take up the majority of Figure 10. These include many objects that are labeled evolved giants. As described in Lucatello et al. (2006), it is possible that their

carbon abundance were higher in the past, but due to dilution by mixing processes are lower now.

### 5.3. Fraction of C-rich stars

One of the most helpful ways for understanding how C-rich stars were formed is determining their relative fraction at different metallicities. Aggregate percentages of C-rich stars ( $[C/Fe] \geq 1.0$ ) with  $[Fe/H]$  values less than a particular metallicity have been reported by a number of authors. As discussed in the Introduction, these estimates range from 25% to 9%. Several reasons for the discrepancies have been identified. Cohen et al. (2005) showed that the CaK and H $\delta$  indices that have been used in combination to derive metallicities by BPS, the HES Christlieb et al. (2002b) and the INT study Allende Prieto et al. (2000), among other others, have C molecular features in the “continuum” sidebands. The effect on the H $\delta$  feature suggests that the star is cooler than it actually is, which translates into a lower  $[Fe/H]$ . The CaK feature also appears to be weaker, which further increases the discrepancy between the measured and the real  $[Fe/H]$ . The  $[C/Fe]$  ratios in these stars are then artificially high. A second effect is the real decline in C abundance as stars move up the red giant branch (Lucatello et al. 2006). Both effects can be ignored for stars with  $T_{\text{eff}} > 5200$  where the CH lines around the CaK feature are insignificant (Cohen et al. 2005) and the depletion of C in red giants has not begun (see Figure 6). Of course, this reduces the sample of stars available for calculating the fraction of C-rich stars, and makes the addition of more metal-poor stars with complete abundances important.

Possible reasons for this study to be biased toward or against finding C-rich stars are the effects of C-richness on metallicity estimators used in this study. In particular, if C-richness makes the star appear more iron-poor than it actually is, then it would have a greater chance of showing up in our study. For the sources for our study, the *ubvy* photometry of Anthony-Twarog et al. (2000) is unaffected by molecular carbon features (Schuster et al. 2004), The INT study (Allende Prieto et al. 2000) used the CaK, CaI line at 4226Å and the hydrogen with a neural network to calculate metallicities. As with BPS, this technique should be relatively unaffected for stars with  $T_{\text{eff}} > 5200\text{K}$ . Finally, we used the UBV photometry of Norris et al. (1999) to identify metal-poor candidates by their UV excesses. To test whether the UBV colors were sensitive to C abundance as well as metallicity, we found UBV photometry for as many CEMP stars as we could, as well as confirmed non-CEMP stars of similar metallicities in the photometric catalogs of Preston et al. (1991), Norris et al. (1999), and Beers et al. (2007). If we confine ourselves again to stars with higher temperatures, we found that very metal-poor carbon-rich stars and carbon-normal metal-poor stars fall in

the same part of the UVB diagram, so we expect our selection based on UV excess to be essentially unaffected by stars of differing  $[C/Fe]$ . The sample size of very metal-poor stars with complete UVB photometry and abundances is small, but the photometric result is consistent with the molecular bands being weaker in the bluer stars. We therefore conclude that our sample of stars with  $T_{\text{eff}} > 5200\text{K}$  is only negligibly affected by bias toward finding carbon-rich stars.

There is one additional effect that must be mentioned. There is increasing observational evidence that the fraction of C-rich stars climbs as  $[Fe/H]$  decreases. Given the apparent dependence of the fraction of stars that are C-rich on  $[Fe/H]$ , a survey that was particularly efficient at finding stars with  $[Fe/H] < -4$  would report a higher C-fraction than one that was not, even if both groups overall studied stars with  $[Fe/H] < -2.0$ . In Figure 11, we plot the metallicity distribution functions at  $[Fe/H] < -2.0$  for BPS, Frebel et al. (2006) and this study. There are clear differences in the MDFs. The BPS and our MDF in this metallicity range peak at  $[Fe/H] \simeq -2.0$ , while the Frebel et al. (2006) MDF has two peaks, the strongest at  $[Fe/H] \simeq -3.0$  and a lower one at  $[Fe/H] \simeq -2.3$ . Also, although our MDF has the same peak range as that of BPS, we do not sample the space below  $[Fe/H] = -3.2$  well, a result of our much smaller sample size. While some of this is likely caused by different metallicity scales, arising, for example, from different temperature scales, that does not explain all the differences in the observed MDFs. These differences will be reflected in the percentage of C-rich stars.

We have directly tested for the effect of differing observational MDFs on derived C-rich fractions. Using the MDFs shown in Figure 11, we have recalculated the C-rich percentage if our sample had the same MDF as Frebel et al. (2006) (because of the small number of stars with  $[Fe/H] < -3$  in our sample, in this example we put all of the stars below this metallicity into the  $[Fe/H] - 3.0$  bin for both MDFs). This was done by first finding the percentage of C-rich stars in each of the bins (0.1 dex in  $[Fe/H]$ ) for our sample. We then applied this percentage to the each respective bin of the Frebel MDF, and recalculated the percentage of C-rich stars with  $[Fe/H] < -2.0$ . We find the fraction of C-rich stars to increase by 3%, a small but noticeable amount. We also carried this out using the BPS MDF in place of the Frebel MDF, and we find that the C-rich percentage increases by 2%. The reason for this becomes clear when examining Figure 11. Both the Frebel and BPS MDFs have a higher percentage of their stars below  $[Fe/H] = -2.75$  compared to ours, and having more stars at lower metallicity will increase the overall C-rich fraction.

To further provide some estimate of the size of the effect, we have selected four possible distributions of the fraction of C-rich objects as a function of  $[Fe/H]$  for  $[Fe/H] < -2.0$ . These are illustrated in Figure 12. The distributions are described below, with  $f(\text{CEMP})$  standing

for the fraction of stars with  $[C/Fe] \geq 1.0$ .

$$\begin{aligned}
 \text{Case 1: } f(\text{CEMP}) &= -0.15 \times [\text{Fe}/\text{H}] - 0.25 \\
 \text{Case 2: } f(\text{CEMP}) &= 0.05 && [\text{Fe}/\text{H}] > -3.0 \\
 &= 0.80 && -3.0 > [\text{Fe}/\text{H}] > -3.2 \\
 &= 0.40 && [\text{Fe}/\text{H}] < -3.2 \\
 \text{Case 3: } f(\text{CEMP}) &= 0.05 && [\text{Fe}/\text{H}] > -3.0 \\
 &= 0.50 && [\text{Fe}/\text{H}] < -3.0 \\
 \text{Case 4: } f(\text{CEMP}) &= 0.04 + 0.06 \times [\text{Fe}/\text{H}] + 0.030 \times [\text{Fe}/\text{H}]^2
 \end{aligned}$$

These cases were mainly motivated by having a lower fraction of CEMP stars at higher metallicity than at lower metallicity. In Case 2 and Case 3, the transition is a sharp jump, while in Case 1 and Case 4, the transition is more gradual. Case 2 includes the possibility that a large number of CEMP-s stars are created at that particular metallicity, if it is possible for a large fraction of lower-mass AGB stars to be created at that metallicity. These are by no means the only possibilities and are merely meant to illustrate the range of CEMP fractions that can occur. The expected fraction of C-rich stars for each case, given the MDF of a particular study are listed in Table 6. The errors were calculated from the standard error of the sample for 1000 Monte Carlo realizations of drawing stars from the given MDFs.

It is clear that including only stars with  $[\text{Fe}/\text{H}] < -2.5$  results in higher fractions than if a more metal-rich ( $[\text{Fe}/\text{H}] < -2.0$ ) cut is used, and comparisons between studies should at the very least be done using the same metallicity cut. Table 6 also illustrates that even if the same metallicity range is used, very different fractions of C-rich stars can be observed for the same underlying distribution. In Case 2, the range is 11% to 29%, an effect that is entirely due to the different MDFs for stars more metal-poor than  $[\text{Fe}/\text{H}] < -2.5$ . Therefore this study’s reported fraction of 12% C-rich stars for  $[\text{Fe}/\text{H}] < -2.0$  (admittedly with large uncertainties) is not incompatible with the higher fractions reported by Marsteller et al. (2005) for the BPS sample for  $[\text{Fe}/\text{H}] < -2.5$ . The fraction of 9% from Frebel et al. (2006) is not duplicated by the current choices for  $f(\text{CEMP})$ . However, because it is also probable that if the fraction of C-rich stars increases with distance from the plane, as reported by Frebel et al. (2006), then the focus of that paper on brighter stars and the focus of this paper on fainter ones, could provide an additional explanation of the offset since we may then expect the  $f(\text{CEMP})$  to have a different form. Therefore, continued work on the fraction of C-rich stars must either adequately sample the MDF or be corrected for its effects to determine an accurate form for the  $f(\text{CEMP})$ , and also must take into account the possible effect of location relative to the galactic plane. Larger sample of stars, for example from the SDSS survey (Marsteller et al. 2006), show promise in providing the most bias-free results in this area.

This research is based in part upon work supported by the National Science Foundation under Grant Number AST-0098617. Any opinions, findings, and conclusions or recommendations expressed in this material are those of the author(s) and do not necessarily reflect the views of the National Science Foundation. The authors wish to recognize and acknowledge the very significant cultural role and reverence that the summit of Mauna Kea has always had within the indigenous Hawaiian community. We are most fortunate to have the opportunity to conduct observations from this mountain.

## REFERENCES

- Allende Prieto, C., Rebolo, R., López, R. J. G., Serra-Ricart, M., Beers, T. C., Rossi, S., Bonifacio, P., & Molaro, P. 2000, *AJ*, 120, 1516
- Anders, E., & Grevesse, N. 1989, *Geochim. Cosmochim. Acta*, 53, 197
- Anthony-Twarog, B. J., Sarajedini, A., Twarog, B. A., & Beers, T. C. 2000, *AJ*, 119, 2882
- Aoki, W., Beers, T. C., Christlieb, N., Norris, J. E., Ryan, S. G., & Tsangarides, S. 2007, *ApJ*, 655, 492
- Aoki, W., Honda, S., Beers, T. C., Kajino, T., Ando, H., Norris, J. E., Ryan, S. G., Izumiura, H., Sadakane, K., & Takada-Hidai, M. 2005, *ApJ*, 632, 611
- Aoki, W., Norris, J. E., Ryan, S. G., Beers, T. C., & Ando, H. 2002a, *ApJ*, 576, L141
- . 2002b, *ApJ*, 567, 1166
- Aoki, W., Ryan, S. G., Norris, J. E., Beers, T. C., Ando, H., & Tsangarides, S. 2002c, *ApJ*, 580, 1149
- Barklem, P. S., Christlieb, N., Beers, T. C., Hill, V., Bessell, M. S., Holmberg, J., Marsteller, B., Rossi, S., Zickgraf, F.-J., & Reimers, D. 2005, *A&A*, 439, 129
- Beers, T. C., & Christlieb, N. 2005, *ARA&A*, 43, 531
- Beers, T. C., Flynn, C., Rossi, S., Sommer-Larsen, J., Wilhelm, R., Marsteller, B., Lee, Y. S., de, N. L., Krugler, J., Deliyannis, C. P., Simmons, A. T., Mills, E., Zickgraf, F.-J., Holmberg, J., Oehag, A., Eriksson, A., Terndrup, D. M., Salim, S., Andersen, J., Nordstrom, B., Christlieb, N., Frebel, A., & Rhee, J. 2007, *ApJS*, 168, 128

- Beers, T. C., Lee, Y., Sivarani, T., Marsteller, B., Krugler, J., Wilhelm, R., Allende Prieto, C., Norris, J., Johnson, J., Ivans, I., Yanny, B., Rockosi, C., Morrison, H., Newberg, H. J., & Knapp, J. 2006, in American Astronomical Society Meeting Abstracts, 168.08–+
- Beers, T. C., Preston, G. W., & Shectman, S. A. 1992, *AJ*, 103, 1987
- Bergbusch, P. A., & Vandenberg, D. A. 1992, *ApJS*, 81, 163
- Bond, H. E. 1980, *ApJS*, 44, 517
- Burris, D. L., Pilachowski, C. A., Armandroff, T. E., Sneden, C., Cowan, J. J., & Roe, H. 2000, *ApJ*, 544, 302
- Cayrel, R., Depagne, E., Spite, M., Hill, V., Spite, F., François, P., Plez, B., Beers, T., Primas, F., Andersen, J., Barbuy, B., Bonifacio, P., Molaro, P., & Nordström, B. 2004, *A&A*, 416, 1117
- Christlieb, N., Bessell, M. S., Beers, T. C., Gustafsson, B., Korn, A., Barklem, P. S., Karlsson, T., Mizuno-Wiedner, M., & Rossi, S. 2002a, *Nature*, 419, 904
- Christlieb, N., Wisotzki, L., & Graßhoff, G. 2002b, *A&A*, 391, 397
- Cohen, J. G., Christlieb, N., McWilliam, A., Shectman, S., Thompson, I., Wasserburg, G. J., Ivans, I., Dehn, M., Karlsson, T., & Melendez, J. 2004, *ApJ*, 612, 1107
- Cohen, J. G., Shectman, S., Thompson, I., McWilliam, A., Christlieb, N., Melendez, J., Zickgraf, F.-J., Ramírez, S., & Swenson, A. 2005, *ApJ*, 633, L109
- Frebel, A., Aoki, W., Christlieb, N., Ando, H., Asplund, M., Barklem, P. S., Beers, T. C., Eriksson, K., Fechner, C., Fujimoto, M. Y., Honda, S., Kajino, T., Minezaki, T., Nomoto, K., Norris, J. E., Ryan, S. G., Takada-Hidai, M., Tsangarides, S., & Yoshii, Y. 2005, *Nature*, 434, 871
- Frebel, A., Christlieb, N., Norris, J. E., Beers, T. C., Bessell, M. S., Rhee, J., Fechner, C., Marsteller, B., Rossi, S., Thom, C., Wisotzki, L., & Reimers, D. 2006, *ApJ*, 652, 1585
- Fujimoto, M. Y., Ikeda, Y., & Iben, I. J. 2000, *ApJ*, 529, L25
- Gratton, R. G., Sneden, C., Carretta, E., & Bragaglia, A. 2000, *A&A*, 354, 169
- Hill, V., Plez, B., Cayrel, R., Beers, T. C., Nordström, B., Andersen, J., Spite, M., Spite, F., Barbuy, B., Bonifacio, P., Depagne, E., François, P., & Primas, F. 2002, *A&A*, 387, 560

- Honda, S., Aoki, W., Ishimaru, Y., Wanajo, S., & Ryan, S. G. 2006, *ApJ*, 643, 1180
- Honda, S., Aoki, W., Kajino, T., Ando, H., Beers, T. C., Izumiura, H., Sadakane, K., & Takada-Hidai, M. 2004, *ApJ*, 607, 474
- Ivans, I. I., Simmerer, J., Sneden, C., Lawler, J. E., Cowan, J. J., Gallino, R., & Bisterzo, S. 2006, *ApJ*, 645, 613
- Johnson, J. A., & Bolte, M. 2002a, *ApJ*, 579, L87
- . 2002b, *ApJ*, 579, 616
- . 2004, *ApJ*, 605, 462
- Kratz, K.-L., Farouqi, K., Pfeiffer, B., Truran, J. W., Sneden, C., & Cowan, J. J. 2007, *ArXiv Astrophysics e-prints*
- Kurucz, R. L., & Bell, B. 1995, *Atomic line list (Kurucz CD-ROM, Cambridge, MA: Smithsonian Astrophysical Observatory, —c1995, April 15, 1995)*
- Lai, D. K., Bolte, M., Johnson, J. A., & Lucatello, S. 2004, *AJ*, 128, 2402
- Lucatello, S., Beers, T. C., Christlieb, N., Barklem, P. S., Rossi, S., Marsteller, B., Sivarani, T., & Lee, Y. S. 2006, *ApJ*, 652, L37
- Lucatello, S., Gratton, R., Cohen, J. G., Beers, T. C., Christlieb, N., Carretta, E., & Ramírez, S. 2003, *AJ*, 125, 875
- Marsteller, B., Beers, T. C., Rossi, S., Christlieb, N., Bessell, M., & Rhee, J. 2005, *Nuclear Physics A*, 758, 312
- Marsteller, B. E., Beers, T. C., Sivarani, T., Rossi, S., Knapp, J., Plez, B., Johnson, J., & Masseron, T. 2006, in *American Astronomical Society Meeting Abstracts*, 242.02–+
- McWilliam, A. 1998, *AJ*, 115, 1640
- McWilliam, A., Preston, G. W., Sneden, C., & Searle, L. 1995, *AJ*, 109, 2757
- Norris, J. E., Ryan, S. G., & Beers, T. C. 1997, *ApJ*, 489, L169+
- . 1999, *ApJS*, 123, 639
- Preston, G. W., Shtetman, S. A., & Beers, T. C. 1991, *ApJS*, 76, 1001



- Rossi, S., Beers, T. C., Sneden, C., Sevastyanenko, T., Rhee, J., & Marsteller, B. 2005, *AJ*, 130, 2804
- Ryan, S. G., Aoki, W., Norris, J. E., & Beers, T. C. 2005, *ApJ*, 635, 349
- Schuster, W. J., Beers, T. C., Michel, R., Nissen, P. E., & García, G. 2004, *A&A*, 422, 527
- Sheinis, A. I., Bolte, M., Epps, H. W., Kibrick, R. I., Miller, J. S., Radovan, M. V., Bigelow, B. C., & Sutin, B. M. 2002, *PASP*, 114, 851
- Sneden, C., Cowan, J. J., Lawler, J. E., Ivans, I. I., Burles, S., Beers, T. C., Primas, F., Hill, V., Truran, J. W., Fuller, G. M., Pfeiffer, B., & Kratz, K.-L. 2003, *ApJ*, 591, 936
- Sneden, C., McWilliam, A., Preston, G. W., Cowan, J. J., Burris, D. L., & Armosky, B. J. 1996, *ApJ*, 467, 819
- Sneden, C. A. 1973, PhD thesis, AA(THE UNIVERSITY OF TEXAS AT AUSTIN.)
- Spite, M., Cayrel, R., Plez, B., Hill, V., Spite, F., Depagne, E., François, P., Bonifacio, P., Barbuy, B., Beers, T., Andersen, J., Molaro, P., Nordström, B., & Primas, F. 2005, *A&A*, 430, 655
- Travaglio, C., Gallino, R., Arnone, E., Cowan, J., Jordan, F., & Sneden, C. 2004, *ApJ*, 601, 864
- Truran, J. W., Cowan, J. J., Pilachowski, C. A., & Sneden, C. 2002, *PASP*, 114, 1293
- Westin, J., Sneden, C., Gustafsson, B., & Cowan, J. J. 2000, *ApJ*, 530, 783

Table 1. Sensitivity of Carbon abundance to Atmospheric Parameters, where the relative change in Carbon is given in dex.

Star ID	$T_{\text{eff}}$ (K)	$\log g$ (dex)	$\xi$ (km s $^{-1}$ )	$\Delta[\text{C}/\text{Fe}]_{T_{\text{eff}}+125 \text{ K}}$	$\Delta[\text{C}/\text{Fe}]_{\log g +0.5 \text{ dex}}$	$\Delta[\text{C}/\text{Fe}]_{\xi +0.5 \text{ km s}^{-1}}$	Total
BD+02 3375*	5926	4.63	1.0	0.08	0.09	0.07	0.14
CS 22183-031	5416	3.31	1.5	0.10	−0.06	0.12	0.16
BS 16928-053	4743	1.61	2.0	0.12	−0.09	0.13	0.16

\* $\log g$  is varied by  $-0.5$  dex for this object because of its already high initial value.

Table 2. Sensitivity of Strontium abundance to Atmospheric Parameters, where the relative change in Strontium is given in dex.

Star ID	$T_{\text{eff}}$ (K)	$\log g$ (dex)	$\xi$ (km s $^{-1}$ )	$\Delta[\text{Sr}/\text{Fe}]_{T_{\text{eff}}+125 \text{ K}}$	$\Delta[\text{Sr}/\text{Fe}]_{\log g +0.5 \text{ dex}}$	$\Delta[\text{Sr}/\text{Fe}]_{\xi +0.5 \text{ km s}^{-1}}$	Total
BD+02 3375*	5926	4.63	1.0	0.04	−0.10	−0.22	0.24
CS 22183-031	5416	3.31	1.5	−0.06	0.09	−0.23	0.25
BS 16928-053	4743	1.61	2.0	−0.13	0.06	−0.32	0.34

\* $\log g$  is varied by  $-0.5$  dex for this object because of its already high initial value.

Table 3. Atmospheric parameters and abundances

Star ID	$T_{eff}$ (K)	$\log g$ (dex)	[Fe/H] (dex)	[Sr/Fe] (dex)	[Ba/Fe] (dex)	[C/Fe] dex	Synthesis [C/Fe] error	Atmosphere [C/Fe] error	Total [C/Fe] error
BD-03 2525	5789	3.60	-1.75	-0.25	-0.37	0.10	0.10	0.16	0.19
BD+02 3375	5926	4.63	-2.25	0.30	-0.01	0.00	0.20	0.14	0.24
BD+23 3130	5224	2.82	-2.59	-0.21	-0.25	0.30	0.10	0.16	0.19
BD+37 1458	5332	3.13	-2.01	0.31	0.00	0.30	0.10	0.16	0.19
HD 6755	5075	2.41	-1.63	0.03	-0.25	-0.00	0.10	0.16	0.19
HD 44007	4773	1.68	-1.89	0.39	-0.18	-0.00	0.10	0.16	0.19
HD 63791	4619	1.34	-1.87	0.12	-0.29	-0.10	0.10	0.16	0.19
HD 74462	4510	1.11	-1.76	0.31	-0.34	-0.20	0.10	0.16	0.19
HD 84937	6312	4.51	-1.91	0.21	-0.07	< 0.10	...	0.14	...
HD 94028	5925	4.63	-1.36	0.36	-0.04	-0.05	0.10	0.14	0.17
HD 115444	4775	1.68	-2.86	0.26	0.34	-0.15	0.10	0.16	0.19
HD 122563	4610	1.32	-2.54	-0.06	-1.01	-0.40	0.10	0.16	0.19
HD 163810	5392	4.73	-1.31	0.11	0.09	-0.50	0.10	0.14	0.17
HD 204543	4570	1.24	-1.98	0.53	0.23	-0.45	0.10	0.16	0.19
BS 16076-006	5614	3.51	-3.00	< -1.50	< -0.56	0.60	0.20	0.16	0.26
BS 16077-007	5958	3.68	-2.82	0.27 <sup>†</sup>	< -0.58	1.00	0.20	0.16	0.26
BS 16080-054	4838	1.83	-2.74	0.59	-0.19	-0.50	0.20	0.16	0.26
BS 16080-093	5120	2.53	-2.73	0.08	0.11	-0.50	0.20	0.16	0.26
BS 16084-160	4762	1.66	-2.93	-1.97	< -1.71	-0.15	0.20	0.16	0.26
BS 16085-050	4882	1.93	-2.88	-1.72	< -1.35	-0.80	0.20	0.16	0.26
BS 16467-062	5219	2.80	-3.79	< -1.21	< -0.09	0.30	0.30	0.16	0.34
BS 16470-092	5948	3.67	-1.83	0.23	-0.42	0.20	0.20	0.16	0.26
BS 16472-018	4946	2.08	-2.46	0.16	-0.09	-0.25	0.20	0.16	0.26
BS 16472-081	4835	1.82	-1.56	0.16	-0.06	-0.15	0.20	0.16	0.26
BS 16477-003	4919	2.02	-3.12	0.12	-0.32	0.30	0.10	0.16	0.19
BS 16543-092	4523	1.14	-2.36	-0.39	-0.58	-1.00	0.20	0.16	0.26
BS 16546-076	4775	1.68	-1.74	0.39	0.10	-0.15	0.10	0.16	0.19
BS 16547-005	4917	2.01	-1.79	0.04	-0.15	-0.10	0.10	0.16	0.19
BS 16547-006	6047	3.72	-2.43	-0.47	-0.43	0.65	0.20	0.16	0.26
BS 16547-025	5197	2.74	-1.62	0.37	0.48	-0.80	0.20	0.16	0.26
BS 16547-099	5856	3.63	-1.34	0.44	0.68	0.20	0.15	0.16	0.22
BS 16550-087	4791	1.72	-3.10	0.80	-0.98	-0.65	0.20	0.16	0.26
BS 16551-058	4937	2.06	-2.01	0.41	0.31	-0.80	0.20	0.16	0.26
BS 16920-017	4854	1.87	-3.02	-0.48	< -1.37	-0.30	0.20	0.16	0.26
BS 16928-053	4743	1.61	-2.87	0.12	-0.75	-0.15	0.15	0.16	0.22
BS 16929-005	5212	2.78	-3.27	0.52	-0.20	1.05	0.15	0.16	0.22
BS 16934-009	4256	0.59	-1.55	0.30	0.22	-0.60	0.20	0.16	0.26
BS 16934-072	6187	3.78	-1.80	-0.20	0.29	0.40	0.20	0.16	0.26
BS 16945-054	5281	2.99	-2.93	-0.32	-0.07	0.10	0.20	0.16	0.26
BS 16972-003	6231	3.80	-2.42	-0.18	-0.30	< 0.65	...	0.16	...
BS 16972-013	5715	3.56	-1.96	0.16	0.11	-0.04	0.20	0.16	0.26
BS 16981-009	5259	2.92	-2.88	-0.77	0.06	0.40	0.15	0.16	0.22
BS 16986-072	4478	1.04	-1.53	0.03	-0.19	-0.45	0.15	0.16	0.22
BS 17139-007	5918	3.66	-2.42	-0.58	-0.57	0.30	0.20	0.16	0.26
BS 17444-032	5960	3.68	-2.43	-0.07	-0.44	< 0.35	...	0.16	...

Table 3—Continued

Star ID	$T_{eff}$ (K)	$\log g$ (dex)	[Fe/H] (dex)	[Sr/Fe] (dex)	[Ba/Fe] (dex)	[C/Fe] dex	Synthesis [C/Fe] error	Atmosphere [C/Fe] error	Total [C/Fe] error
BS 17446-025	5960	3.68	-2.38	-0.52	-0.82	< 0.50	...	0.16	...
BS 17570-090	5924	3.66	-2.60	-0.80	< -1.72	< 0.30	...	0.16	...
BS 17576-002	6203	3.78	-1.38	0.38	-0.09	0.40	0.10	0.16	0.19
BS 17576-071	6200	3.79	-1.72	0.17	-0.12	0.15	0.20	0.16	0.26
BS 17585-080	4630	1.36	-1.38	-0.12	-0.53	-1.00	0.15	0.16	0.22
CS 22166-016	5388	3.26	-2.47	0.27	-0.19	0.25	0.10	0.16	0.19
CS 22174-012	4934	2.06	-2.52	-0.48	-0.90	-0.70	0.20	0.16	0.26
CS 22180-005	5851	3.63	-1.99	0.19 <sup>†</sup>	0.03	0.30	0.10	0.16	0.19
CS 22183-015	5178	2.69	-3.17	1.22 <sup>†</sup>	1.77	2.10	0.20	0.16	0.26
CS 22183-031	5416	3.31	-2.71	0.16	0.46	0.35	0.10	0.16	0.19
CS 22185-007	5193	2.73	-2.45	-0.45 <sup>†</sup>	-0.46	0.25	0.10	0.16	0.19
CS 22190-007	6013	3.71	-2.02	0.62	0.91	0.00	0.20	0.16	0.26
CS 22878-101	4789	1.72	-2.93	-0.07	-0.53	-0.45	0.10	0.16	0.19
CS 22880-086	5457	3.37	-2.42	0.08	-0.74	0.20	0.20	0.16	0.26
CS 22883-020	6099	3.74	-2.02	-0.38	-0.75	< 0.40	...	0.16	...
CS 22892-052	4854	1.87	-2.99	0.79	1.32	1.00	0.10	0.16	0.19
CS 22893-010	5528	3.44	-2.38	-0.02 <sup>†</sup>	< -1.00	0.30	0.20	0.16	0.26
CS 22898-027	5750	3.58	-2.29	1.12	2.16	1.45	0.10	0.16	0.19
CS 22944-032	5528	3.44	-2.64	0.44 <sup>†</sup>	-0.58	0.65	0.20	0.16	0.26
CS 22949-029	6244	3.81	-1.70	-0.45 <sup>†</sup>	...	0.55	0.20	0.16	0.26
CS 22949-048	4828	1.81	-2.90	-1.10	< -1.38	-0.20	0.10	0.16	0.19
CS 22950-153	5293	3.02	-2.10	0.25	-0.25	-0.15	0.20	0.16	0.26
CS 22957-022	5075	2.41	-3.02	-0.28	-0.89	0.30	0.15	0.16	0.22
CS 22962-006	6325	4.51	-2.25	< -1.42	< -0.43	< 0.50	...	0.14	...
CS 22963-004	5803	3.61	-3.03	< -0.97	< -0.27	< 0.95	...	0.16	...
CS 22965-016	4904	1.99	-2.59	0.09 <sup>†</sup>	< -1.07	-0.70	0.20	0.16	0.26
CS 22965-029	5467	3.38	-2.31	0.61	0.16	-0.60	0.20	0.16	0.26
CS 29497-040	5487	3.41	-2.80	< -1.35	< -0.89	0.35	0.20	0.16	0.26
CS 29502-092	5114	2.51	-2.92	-0.18	-0.92	1.15	0.10	0.16	0.19
CS 29510-008	5577	3.48	-1.69	0.14	-0.24	0.15	0.10	0.16	0.19
CS 29510-058	5192	2.73	-2.51	0.26	-0.14	0.50	0.10	0.16	0.19
CS 29517-025	5647	3.53	-2.19	0.74 <sup>†</sup>	0.71	-0.35	0.20	0.16	0.26
CS 30306-082	5598	3.50	-2.60	-0.25 <sup>†</sup>	-0.41	0.25	0.20	0.16	0.26
CS 30306-110	6056	3.72	-1.85	-0.85 <sup>†</sup>	-0.65	0.05	0.25	0.16	0.30
CS 30306-126	5812	3.61	-1.93	-0.67	-0.58	-0.05	0.20	0.16	0.26
CS 30311-050	5710	3.56	-1.51	-0.09	-0.12	0.15	0.15	0.16	0.22
CS 30315-093	5638	3.52	-2.56	-0.14	-0.52	-0.05	0.20	0.16	0.26
CS 30320-006	5661	3.53	-1.89	-0.11	-0.61	-0.10	0.20	0.16	0.26
CS 30320-069	6119	3.75	-2.02	-0.58 <sup>†</sup>	< -0.62	0.20	0.20	0.16	0.26
CS 30325-028*	4887	1.95	-2.79	0.36	-0.43	0.55	0.10	0.16	0.19
CS 30329-078	5475	3.39	-1.77	0.12	0.09	0.05	0.10	0.16	0.19
CS 30329-129	5467	3.37	-2.41	0.01	-0.60	0.15	0.15	0.16	0.22
CS 30331-018	5379	3.24	-1.77	0.32	0.02	0.00	0.20	0.16	0.26
CS 30332-114	5851	3.63	-1.85	-0.25	-0.31	0.15	0.20	0.16	0.26
CS 30338-119	5611	3.50	-1.82	-0.33	-0.60	0.05	0.20	0.16	0.26

Table 3—Continued

Star ID	$T_{eff}$ (K)	$\log g$ (dex)	[Fe/H] (dex)	[Sr/Fe] (dex)	[Ba/Fe] (dex)	[C/Fe] dex	Synthesis [C/Fe] error	Atmosphere [C/Fe] error	Total [C/Fe] error
CS 31060-030	5682	3.55	−1.68	0.13	−0.83	0.15	0.15	0.16	0.22
CS 31060-043	5452	3.36	−2.06	0.36	0.79	0.05	0.15	0.16	0.22
CS 31061-062	5465	3.38	−2.62	−0.13	−0.22	< −0.25	...	0.16	...
CS 31062-050	5313	3.08	−2.65	1.40	2.37	1.70	0.20	0.16	0.26
CS 31069-064	5468	3.38	−2.19	−0.56	−0.90	0.20	0.15	0.16	0.22
CS 31070-058	4864	1.89	−2.29	0.14	−0.21	0.15	0.10	0.16	0.19
CS 31078-018	5106	2.49	−3.02	0.12	0.13	0.60	0.10	0.16	0.19
CS 31082-001	4893	1.96	−2.78	0.68	1.22	0.30	0.10	0.16	0.19
CS 31085-024	4931	2.05	−3.30	−0.95	< −1.32	0.05	0.15	0.16	0.22
CS 31088-083	5386	3.26	−1.99	0.19	−0.06	0.10	0.10	0.16	0.19

\*The value of [Ba/Fe] was incorrectly given as −1.62 in Paper I.

†The error from the synthetic fit on these objects was  $\sim 0.35$  dex

Table 4. [C/Fe] comparisons with previous studies.

Star ID	[C/Fe] this study	[C/Fe] literature	Ref.
BD+37 1458	0.30	0.14	1
HD 6755	0.00	−0.07	1
HD 74462	−0.20	−0.50	1
HD 94028	−0.05	−0.07	1
HD 115444	−0.15	−0.41	2
HD 122563	−0.45	−0.41	3
HD 204543	−0.70	−0.58	1
BS 16080-054	−0.50	−0.10	4
BS 16084-160	−0.15	0.10	4
BS 16467-062	0.30	0.25	3
BS 16477-003	0.30	0.34	3
BS 16928-053	−0.15	−0.23	2
BS 16929-005	1.05	0.92	2
CS 22183-031	0.35	0.42	2
CS 22878-101	−0.45	−0.29	3
CS 22892-052	1.00	0.89	3
CS 22898-027	1.45	1.90	5
CS 22949-048	−0.20	0.16	5
CS 30325-028	0.55	0.60	4
CS 31082-001	0.30	0.21	3

References. — (1) Gratton et al. (2000); (2) Honda et al. (2004); (3) Cayrel et al. (2004); (4) Aoki et al. (2005); (5) McWilliam et al. (1995)

Table 5. [Sr/Fe] comparisons with previous studies.

Star ID	[Sr/Fe] this study	[Sr/Fe] literature	Ref.
HD 115444	0.26	0.04	1
HD 122563	−0.06	−0.26	2
BS 16080-054	0.59	0.25	3
BS 16084-160	−1.97	−2.34	3
BS16085-050	−1.72	−1.71	1
BS16928-053	0.12	−0.23	1
BS16929-005	0.52	0.28	1
CS22183-031	0.16	0.10	1
CS 22878-101	−0.07	−0.50	4
CS 22892-052	0.79	0.63	5
CS 22898-027	1.12	0.97	4
CS 22949-048	−1.10	−1.47	4
CS 30325-028	0.36	0.27	3
CS 31082-001	0.68	0.65	6

References. — (1) Honda et al. (2004); (2) Honda et al. (2006); (3) Aoki et al. (2005); (4) McWilliam et al. (1995); (5) Sneden et al. (2003); (6) Hill et al. (2002)



Table 6. Predicted Fraction of  $[C/Fe] \geq 1$  Stars for Different Studies

[C/Fe] dist.	BPS	error	F06	error	This Study	error
$[Fe/H] < -2.0$						
Case 1	0.14	0.02	0.15	0.03	0.12	0.05
Case 2	0.15	0.01	0.19	0.02	0.08	0.04
Case 3	0.12	0.01	0.15	0.02	0.07	0.04
Case 4	0.20	0.02	0.21	0.03	0.18	0.06
$[Fe/H] < -2.5$						
Case 1	0.18	0.03	0.19	0.04	0.18	0.05
Case 2	0.24	0.02	0.29	0.03	0.11	0.04
Case 3	0.19	0.02	0.21	0.03	0.10	0.04
Case 4	0.24	0.03	0.26	0.04	0.23	0.06

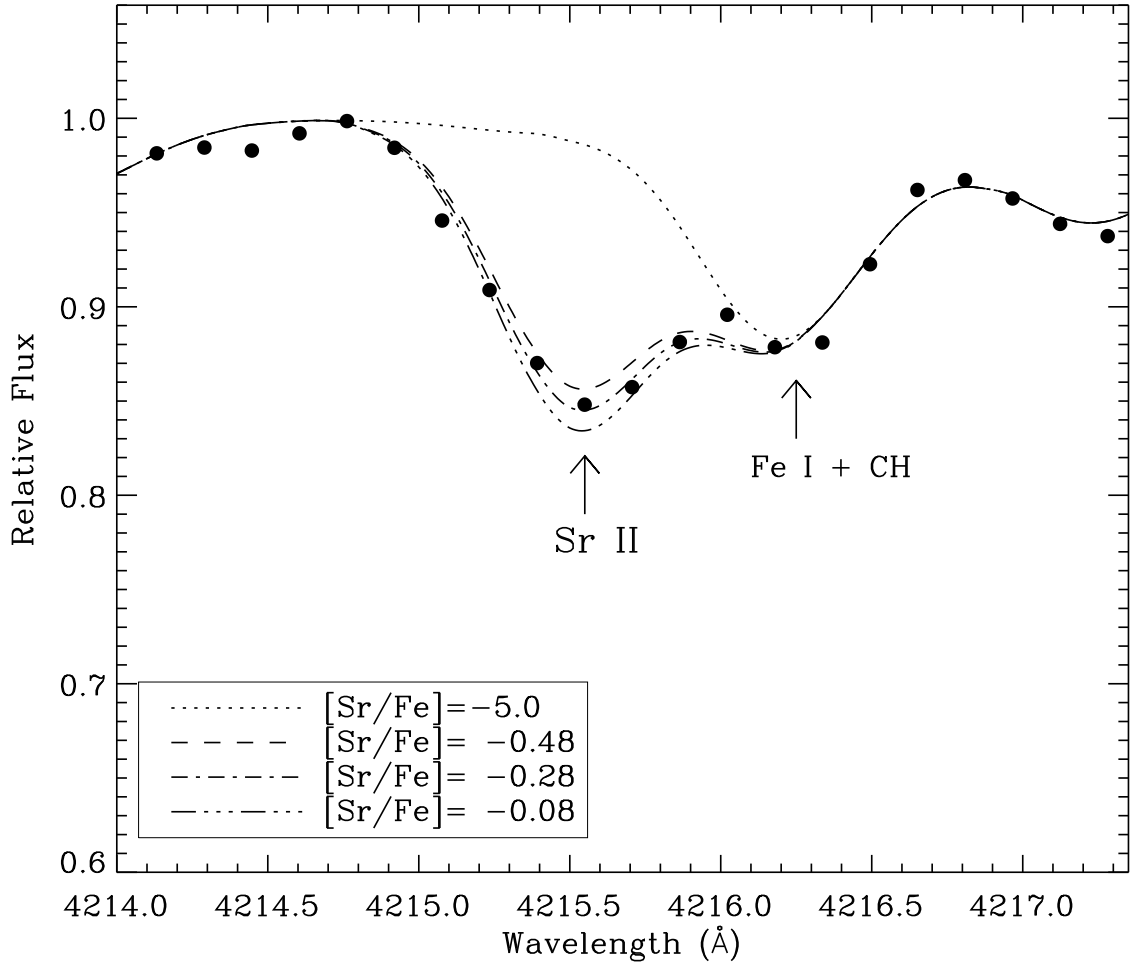


Fig. 1.— Example of the synthesis for Sr II in the star CS 22957-022. The filled circles show the observed spectrum.

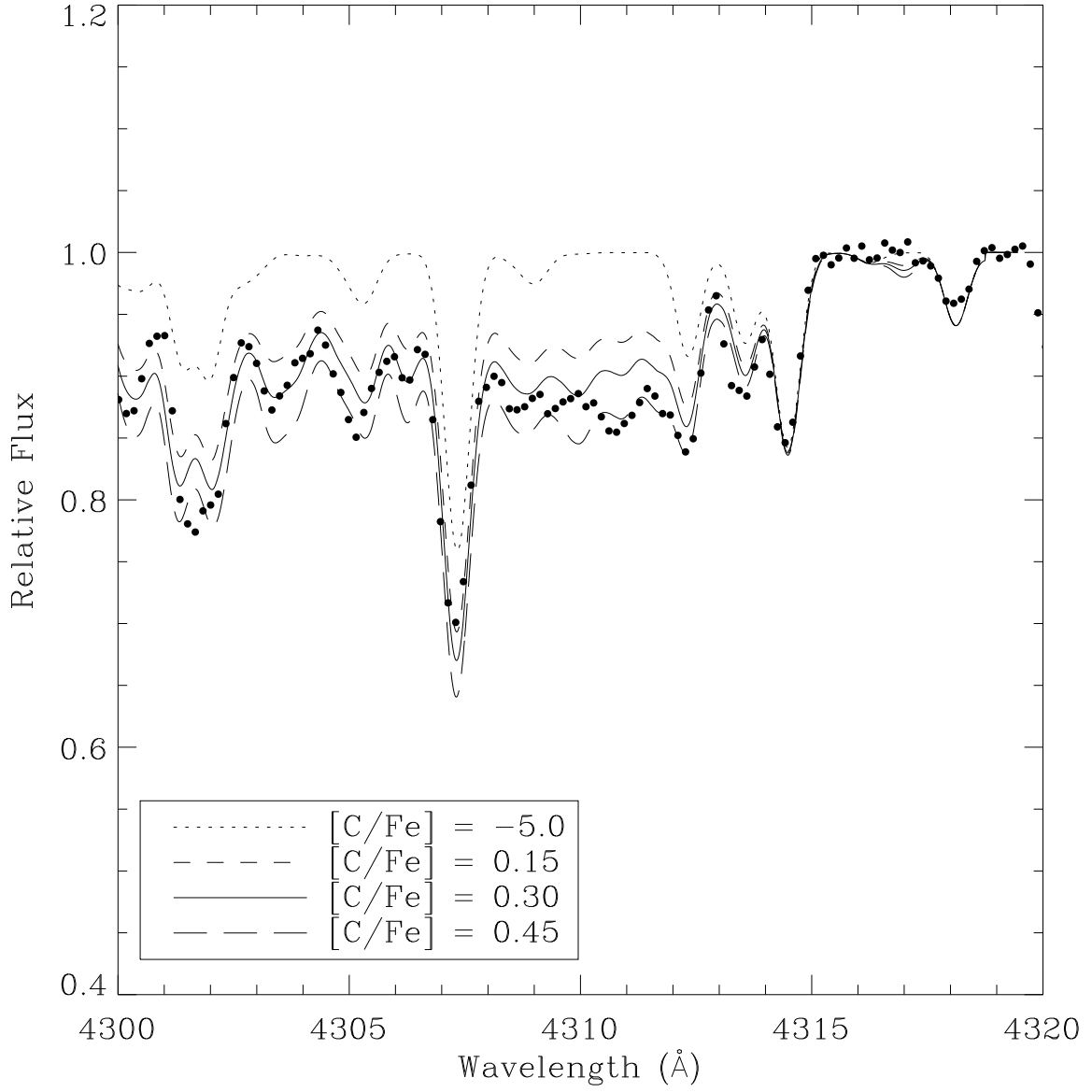


Fig. 2.— Example of G-band synthesis for the star CS 22957-022. The filled circles show the observed spectrum.

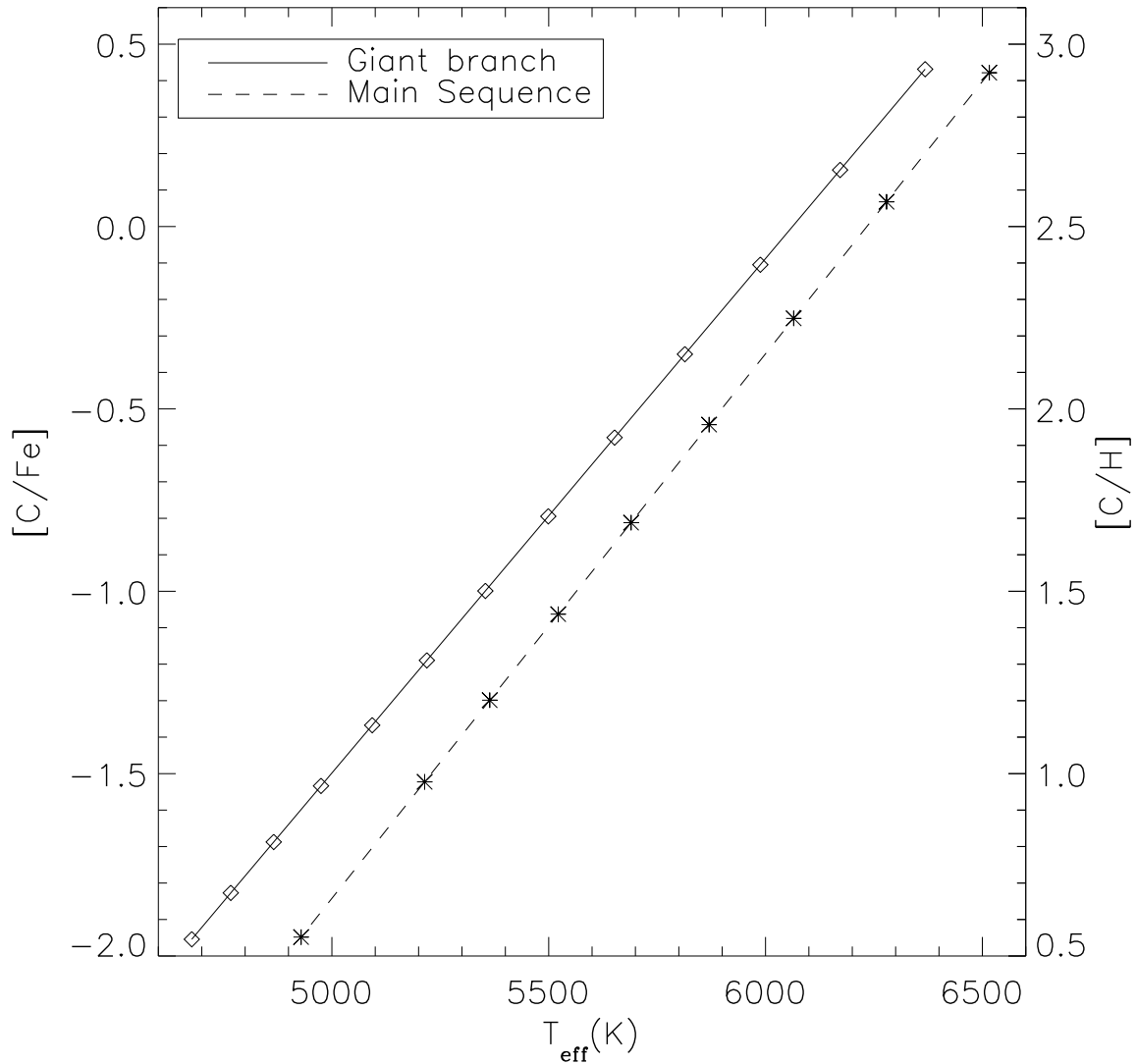


Fig. 3.— Our estimated sensitivity limit to detecting  $[C/Fe]$  in our stars. The value for  $[C/Fe]$  must be above the line at a given temperature to determine more than an upper limit. For increasing temperature, the *loggs* of the giants range from 1.45 to 3.87, and the *loggs* for the main sequence line range from 4.8 to 4.42. The plot shown is for a star with  $[Fe/H]=-2.5$ .

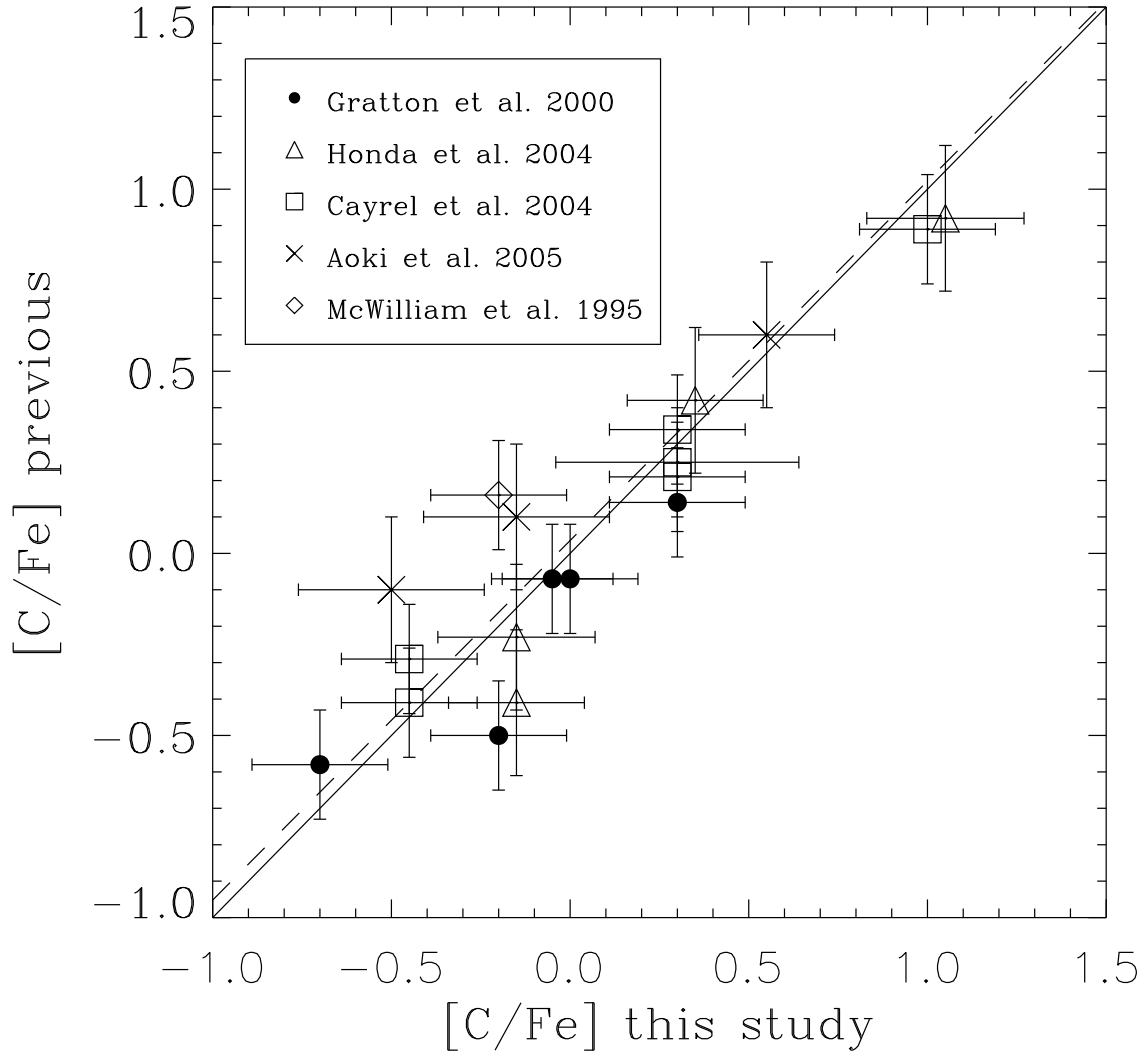


Fig. 4.— A comparison of previous  $[C/Fe]$  measurements with this study. There is a slope of 0.99 to the best fit line (the dashed line) The 1-1 line is shown as the solid line.

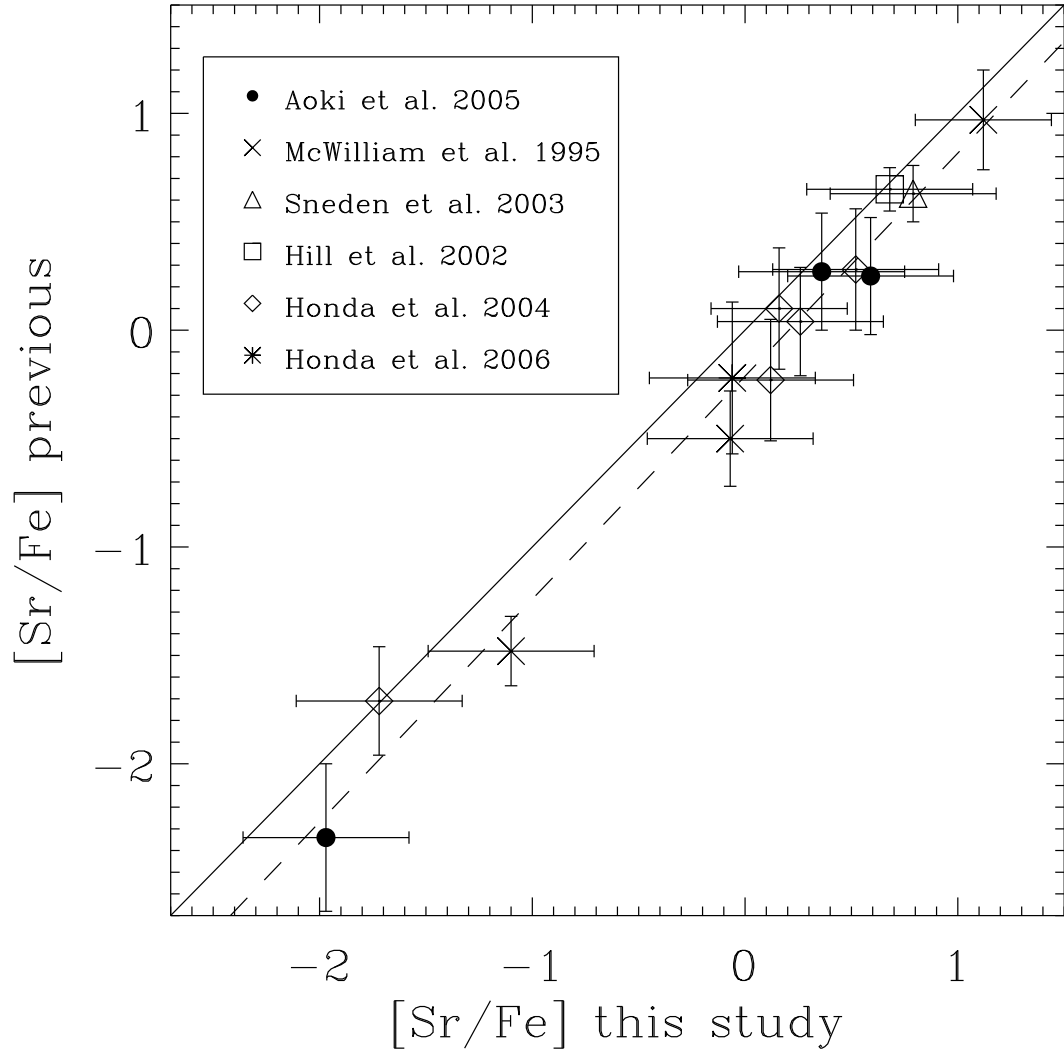


Fig. 5.— A comparison of previous  $[\text{Sr}/\text{Fe}]$  measurements with this study. The best fit line (the dashed line) has a slope of 1.03.

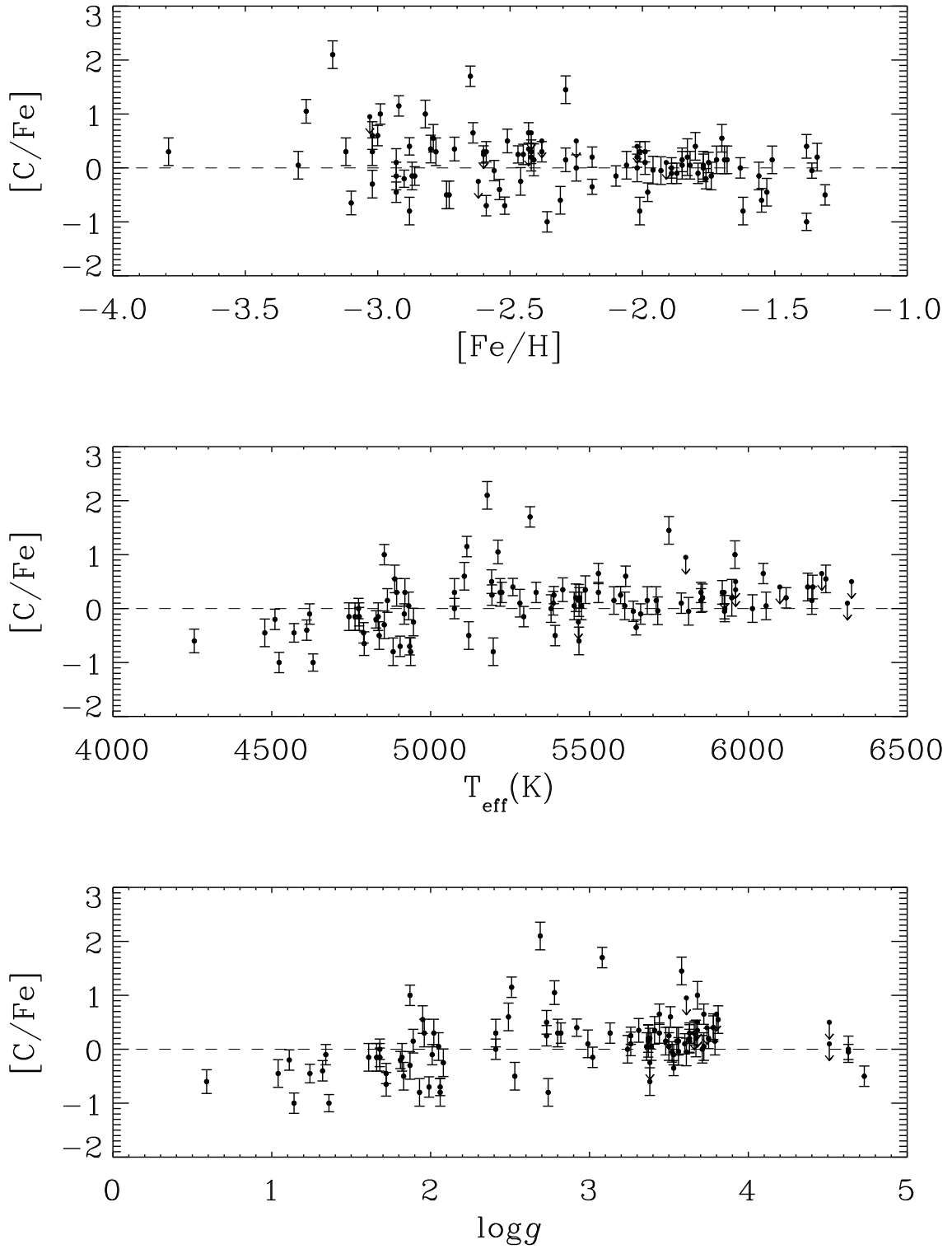


Fig. 6.— Plots of  $[C/Fe]$  versus  $[Fe/H]$ ,  $T_{\text{eff}}$ , and  $\text{logg}$ .

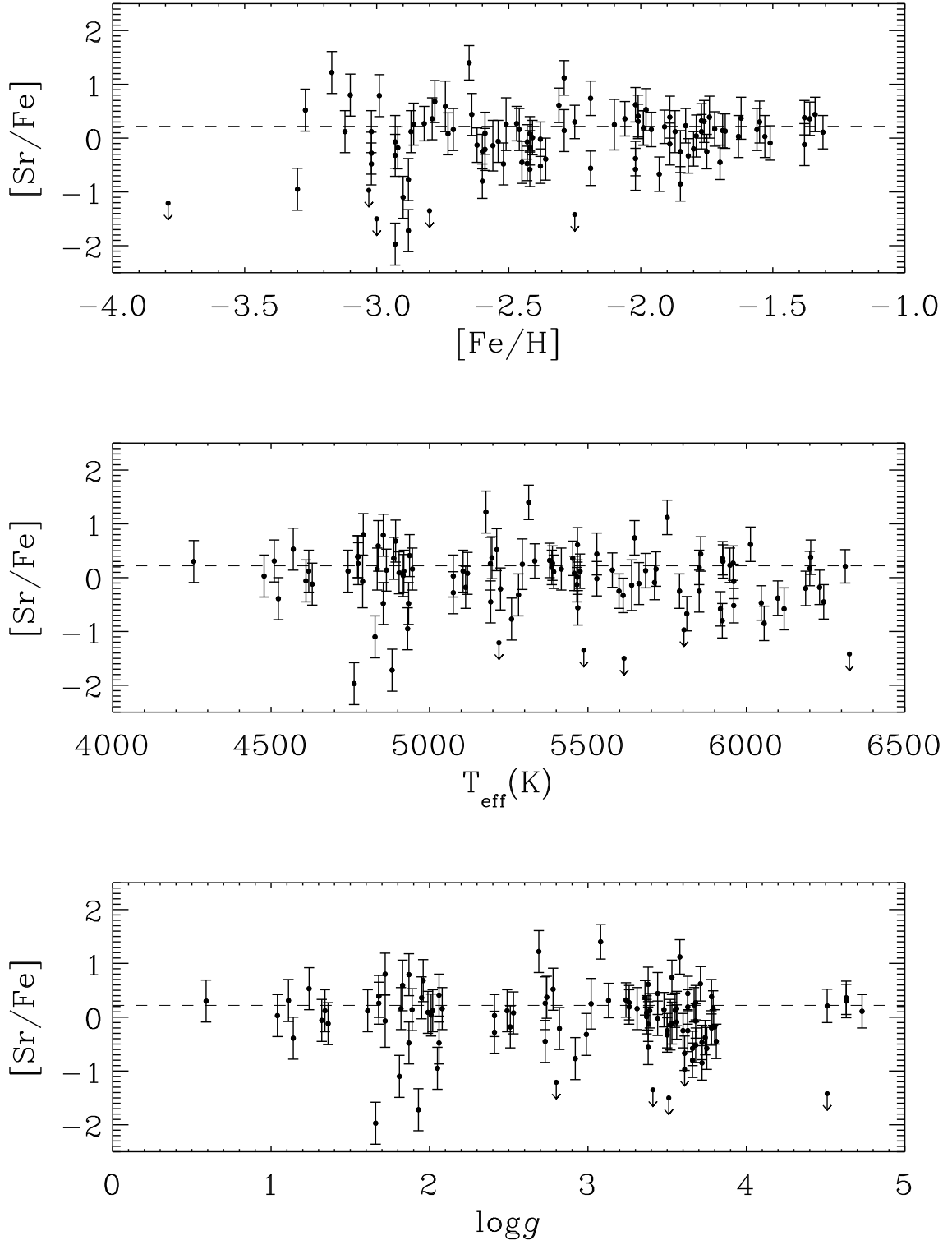


Fig. 7.— Plots of  $[Sr/Fe]$  versus  $[Fe/H]$ ,  $T_{\text{eff}}$ , and  $\text{logg}$ .



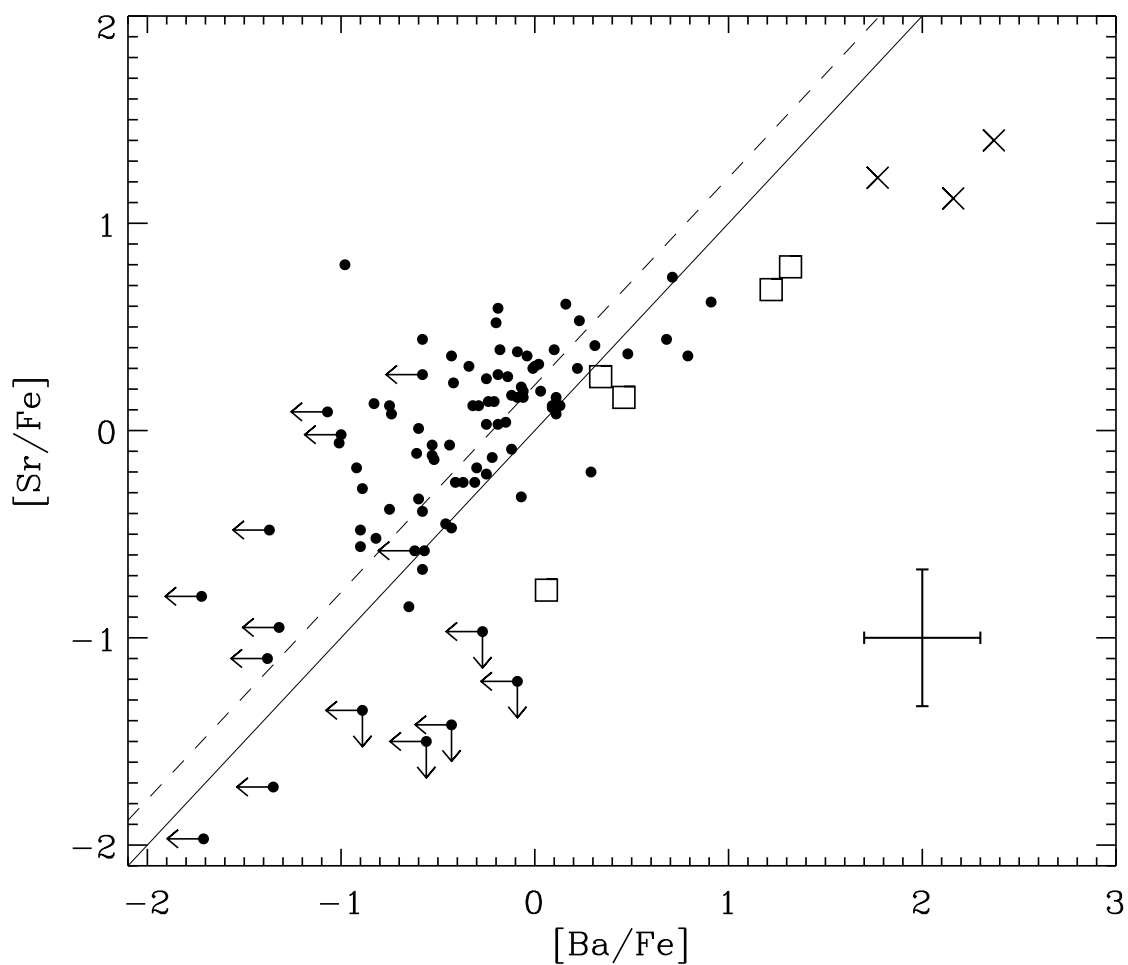


Fig. 8.— A plot of  $[\text{Ba}/\text{Fe}]$  vs.  $[\text{Sr}/\text{Fe}]$ . The one-to-one value is shown as the solid line. The dashed line is the one-to-one line offset by 0.23 dex. A representative error bar is shown in the lower right. Known r-process enhanced stars are plotted with a square symbol, and known s-process enhanced stars are plotted with the ‘x’ symbol. They are HD 115444, BS 16981-009, CS 22183-015, CS 22183-031, CS 22892-052, CS 22898-027, CS 31062-050, and CS 31082-001.

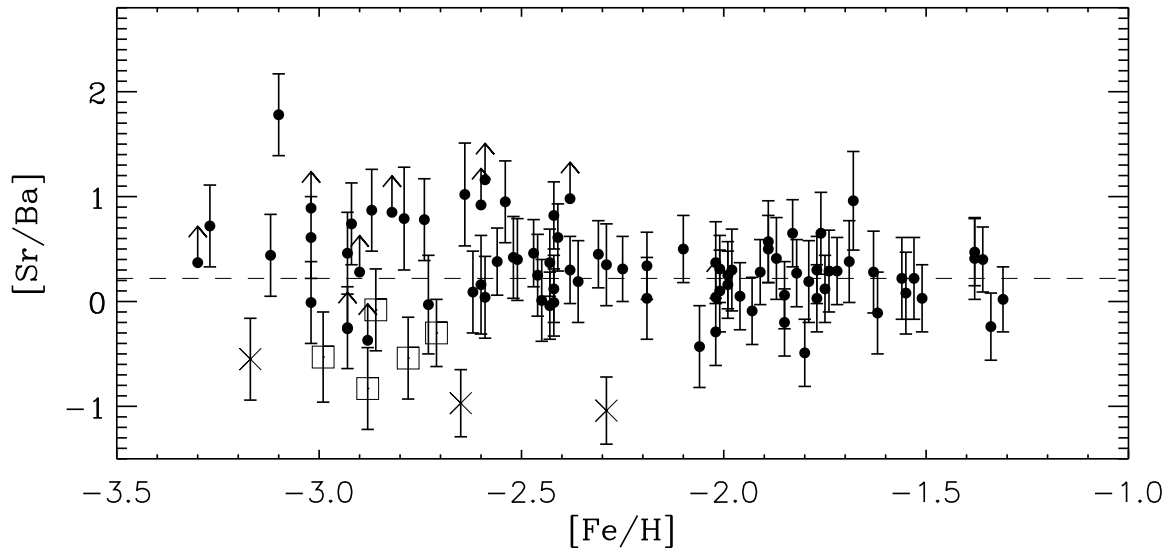


Fig. 9.— Here we plot  $[Sr/Ba]$  as it varies over our range of  $[Fe/H]$ . It is a clear offset above zero for the average of  $[Sr/Ba]$ . The scatter also noticeably increases below  $[Fe/H] -2.0$ . The symbols are the same as in the previous figure.

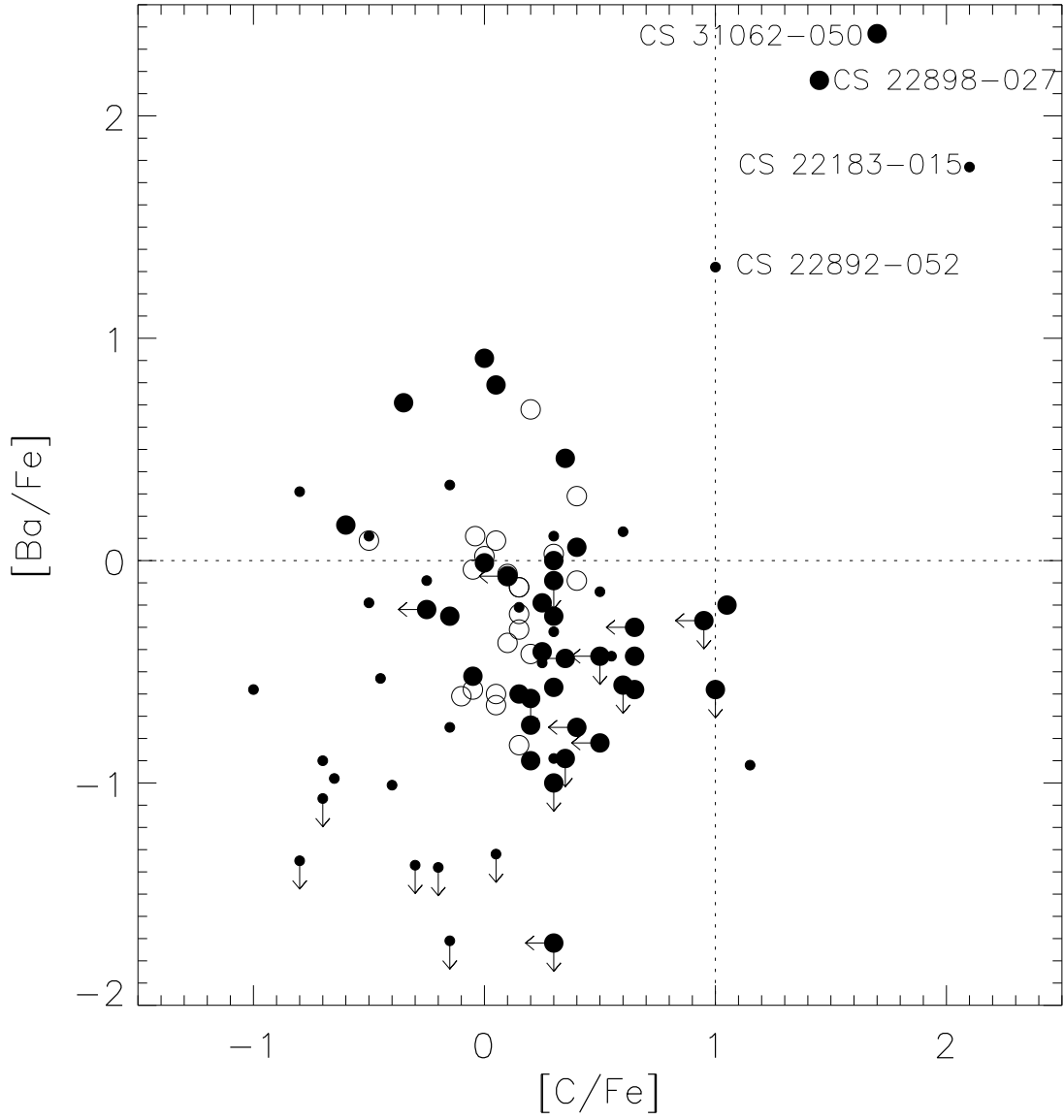


Fig. 10.— Plot of  $[Ba/Fe]$  versus  $[C/Fe]$ . The filled circles represent stars with  $[Fe/H] < -2.0$ . The large circles represent stars with  $T_{eff} \geq 5200K$ , and the small circles stars with  $T_{eff} < 5200K$ .

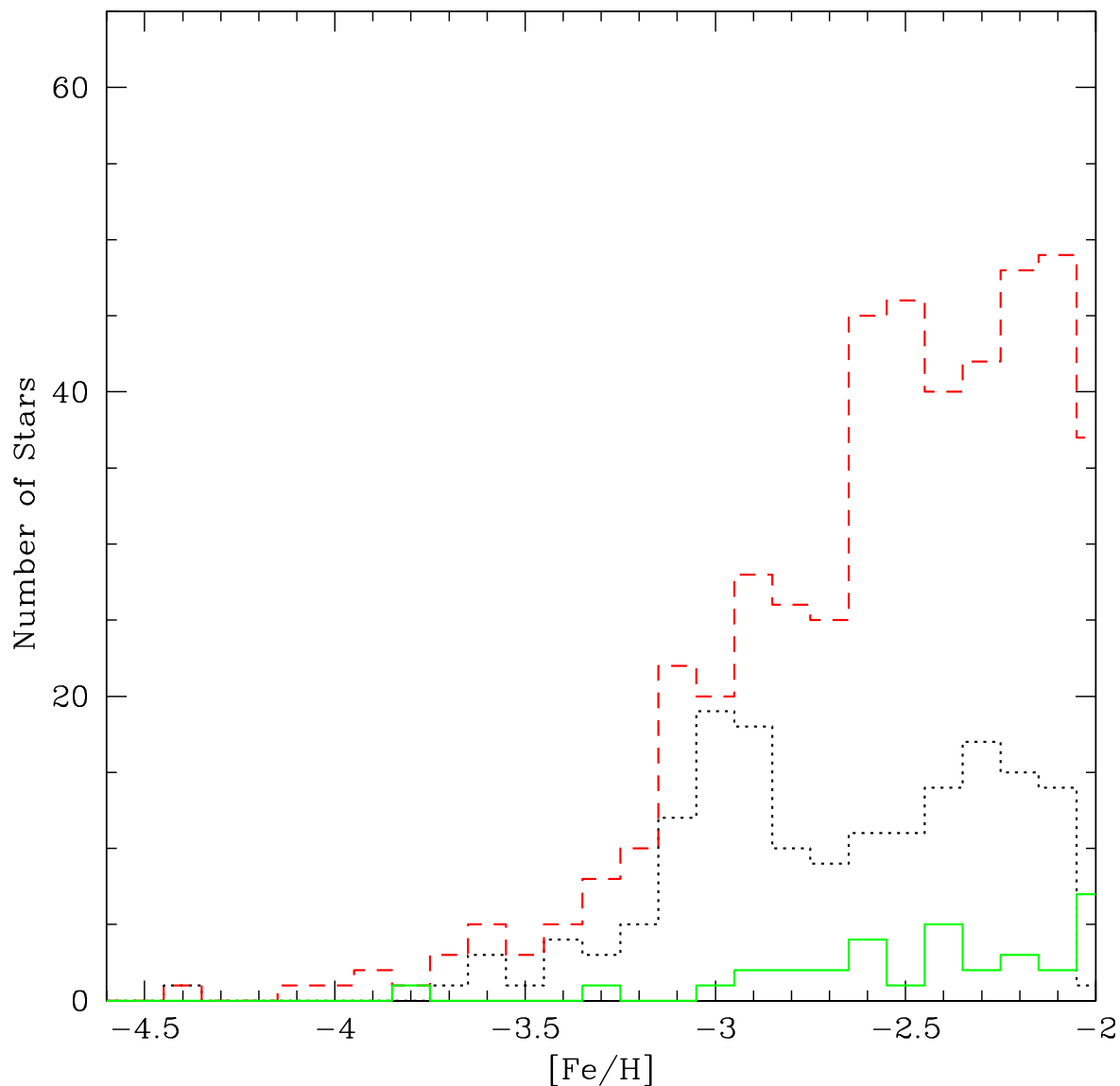


Fig. 11.— The metallicity distribution function for BPS (dashed line), Frebel et al. (2006) (dotted line) and this study (solid line) for all stars with  $[\text{Fe}/\text{H}] < -2.0$ . For this study, the sample was also restricted to stars with  $T_{\text{eff}} > 5200\text{K}$ . The other samples had C-rich fractions quoted for the entire sample, so they were not restricted in  $T_{\text{eff}}$ . See the electronic edition of the Journal for a color version of this figure.

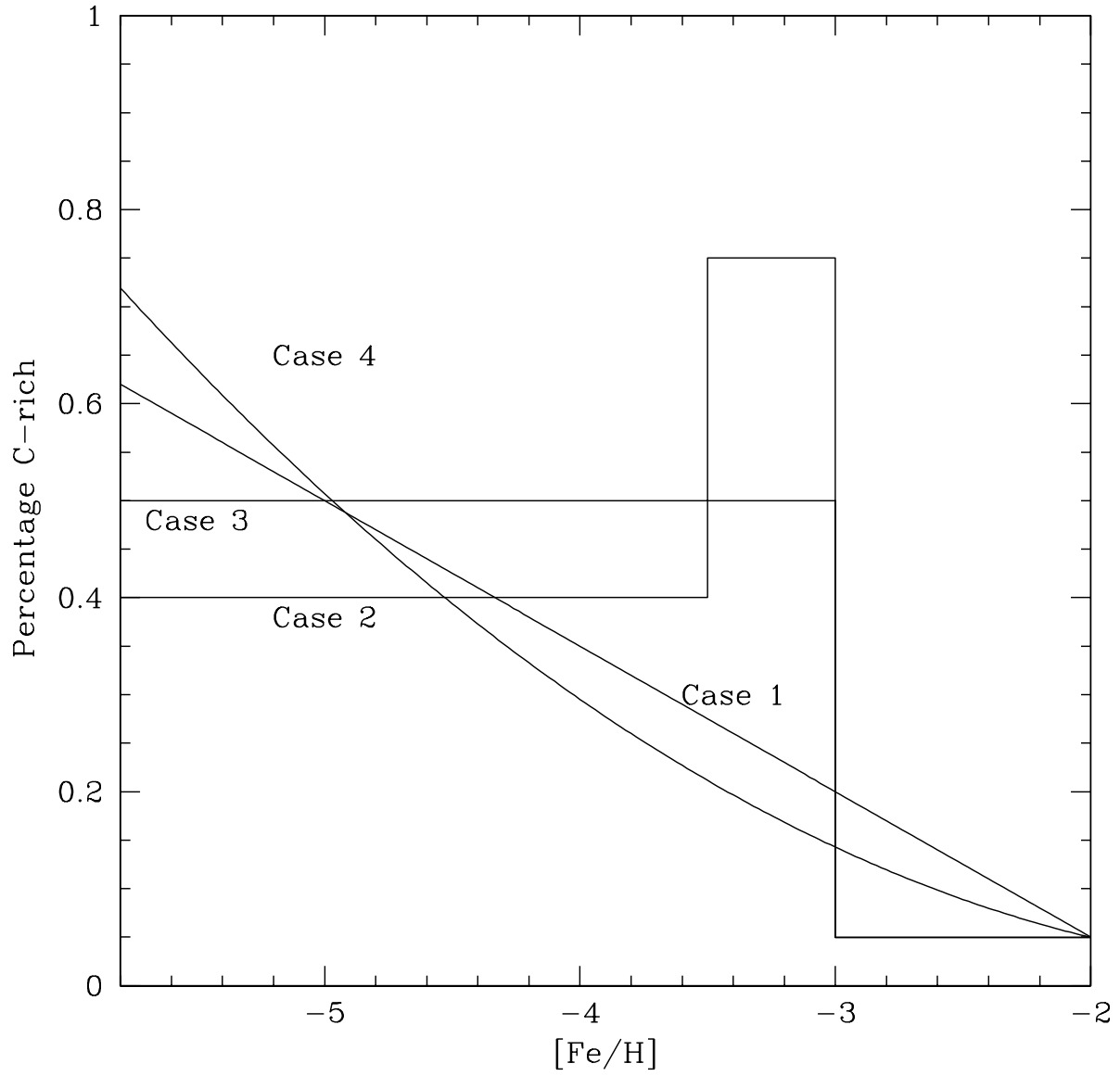


Fig. 12.— Four examples of possible distributions of C-rich stars vs. [Fe/H].